Real Time Control of Shaking Table for the Simulation of Structure-Base Interaction During Earthquakes

REPORT OF RESEARCH PROJECT
1998 GRANT-IN-AID FOR EXPLORATORY RESEARCH
(No. 09875109)
The Ministry of Education, Science, Sports and Culture

March, 1999

Kazuo KONAGAI
Institute of Industrial Science
University of Tokyo

REPORT OF RESEARCH PROJECT
1998 GRANT-IN-AID FOR EXPLORATORY RESEARCH

Project No. **09875109**

Title of project:

REAL TIME CONTROL OF SHAKING TABLE FOR THE SIMULATION OF STRUCTURE-BASE INTERACTION DURING EARTHQUAKES

(地震時の被加振構造物と加振を与える側の動的相互作用を反映した振動台制御手法の開発)

Head investigator: **Kazuo KONAGAI**

Grant-in-aid: 1,100,000 yen, 1997
1,100,000 yen, 1998

Publication list (Peer reviewed):

1) Konagai, K. and T. Nogami: Simulation of Soil-Structure Interaction on a Shaking Table, Numerical and Physical Modeling for Dynamic Soil/Structure Interaction Phenomenon, Logan, Utah, *Geotechnical Special Technical Publication*, **64**, ASCE, 91-106, 1997.
2) Konagai, K., A. Mikami and T. Nogami: Simulation of Soil-Structure Interaction Effects in Shaking Table Tests, Geotechnical Earthquake Engineering and Soil Dynamics 1998, Seattle, *Geotechnical Special Technical Publication*, ASCE, **75(1)**, 482-493, 1998.
3) Konagai, K. and T. Nogami: Analog circuit to simulate dynamic soil-structure interaction in shake table test, *International Journal of Soil Dynamics and Earthquake Engineering*, **17(5)**, 279-287, 1998.
4) Konagai, K., T. Nogami, T., Katsukawa, T., Suzuki and A., Mikami: Real Time Control of Shaking Table for Soil-Structure Interaction Simulation, *Jour. of Structural Mechanics and Earthquake Engineering, JSCE*, **598/I-44**, 203-210, 1998 (in Japanese).
5) Konagai, K., O., Uemura, T., Katsukawa and T., Suzuki: Real Time Simulation of Soil-Structure Interaction Effects on Shaking Tables, Proc., 10th Japan Earthquake Engineering Symposium, **E1-13**, 1647-1652, 1998.
6) Konagai, K., R. Ahsan and D., Maruyama: Simple Expression of the Dynamic Stiffness of Grouped Piles in Sway Motion, *International Jour., Earthquake Engineering*, under review.

PREFACE

Model experiments on a shaking table are quite useful for identification of important phenomena and verification of predictive theories regarding dynamic behavior of a prototype structure subjected to an earthquake; and a shaking table is, in general, controlled so that it follows closely the input *free-field* motion. In reality, however, a structure interacts with its foundation on or in the ground, and responds differently. This interaction thus causes the motion of the ground at the structure's base to deviate from the free-field motion. This effect may be partly incorporated by filling up a bin on the table with actual prototype soil and by putting a model on it. This method is particularly useful when non-linear features of the soil in the vicinity of a structure must be considered. But the process of preparing a soil model is rather difficult; and if prepared, it still can not allow for the effect of wave-dissipation into an infinite soil medium existing in the field.

Shaking tables of many sizes have been used so far. Some are quite large, allowing models with dimensions of several meters to be shaken. However, they are not always large enough for all structural models of interest to be tested. Within the finite base size of a shaking table and within the limit of its dynamic loading capacity, not the whole structure but just one part of it, like some devices for vibration reduction, can be tested. In this case also, the input motion to the model's base must be affected by the presence of the model.

The purpose of this project was to develop a method for controlling a shaking table so that the soil-structure or base-structure interaction effect is incorporated. In order for the interaction effect to be reflected in a shaking table test, the signal equivalent to the further displacement induced by the interaction is added in real-time to the input ground or base motion. This method, therefore, requires a device that can generate the signals corresponding to the base-structure interaction motions. To all intents and purposes, the expression of base stiffness must be simple enough for the device to loose no time in responding to the input force, and producing the base-structure interaction motion. Moreover, real-time adjustment of the shaking table's motion is definitely a prerequisite for the present method, and one cannot do it through iterative trials.

As is the case of many reports, this report is an outgrowth of different peer-reviewed papers published in both domestic and international journals. Chapters in this report are, thus, based on these papers. However, they were so arranged that the outline of this study, and eventually, the remaining problems would be brought in full relief. Acknowledgment here may be in order. I am indebted to the many people whose

suggestions and criticisms have helped me with this project, especially, Dr. Toyoaki Nogami, Professor, Cincinnati University, Dr. Takeyasu Suzuki and Mr. Tota Katsukawa, Technical Research & Development Inst., Kumagai Gumi, Co., Ltd. I should like to thank the students at Konagai Lab., IIS, University of Tokyo, especially, Mr. Osamu Uemura, Mr. Raquib Ahsan, and Mr. Daisuke Maruyama who have conducted difficult experiments and numerical simulations. Dr. Atsushi Mikami, Research Associate, and Mr. Toshihiko Katagiri, technician at Konagai Lab., have devotedly tried out some new ideas. Though their methods are not refined enough to be published yet, they will certainly contrive for better control of shaking tables. Lastly, grateful acknowledgment is made to Ms. Yasuko Takahashi for her help in preparing figures and tables.

K.K.

Roppongi, Tokyo
March, 1999

CONTENTS

Chapter 1

SIMULATION OF SOIL-STRUCTURE INTERACTION EFFECT ON SHAKING TABLES

1.1. TWO PRIMARY CAUSES OF SOIL-STRUCTURE INTERACTION

In this discussion, the multi-step method is used to describe the two primary causes of soil-structure interaction - the inability of the foundation to match the free-field deformation, and the effect of the dynamic response of the superstructure on the movement of its supporting soil-foundation system. A soil-structure system is divided into two substructures, the superstructure and the unbounded soil extending to infinity; the latter includes an embedded foundation as illustrated in **Fig. 1.1**. The displacement of the soil due to an earthquake, which is not affected by the presence of the foundation,

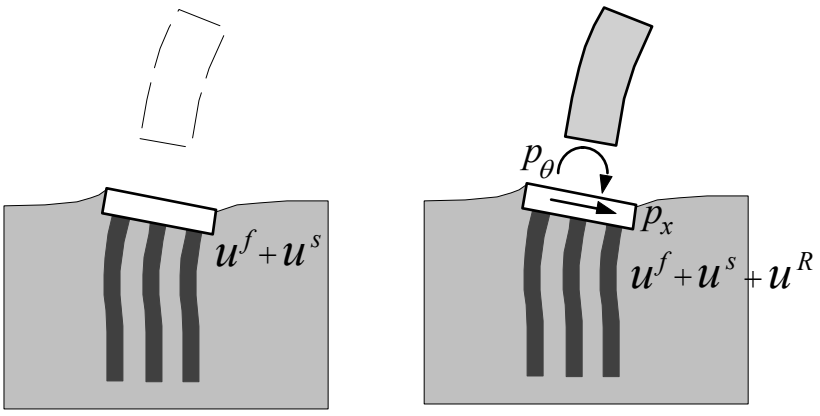

Fig. 1.1 Two primary causes of soil-structure interaction

is referred to as the free-field motion, $\{\mathbf{u}^f\}$. The foundation embedded in the soil deposit, however, will not follow the free-field deformation pattern. This deviation of the displacements from the free-field soil displacements, $\{\mathbf{u}^f\}$, is denoted by $\{\mathbf{u}^s\}$. The mass of the super-structure then causes it to respond dynamically, and the forces, $\{\mathbf{p}\}$, transmitted to the lower soil-foundation substructure will produce further deformation of the soil, $\{\mathbf{u}^R\}$ (***inertia interaction***). The inertia interaction effect would not occur in a fixed base structure. Thus, the displacements of soil, $\{\mathbf{u}\}$, are eventually expressed by the following equation as:

$$\{\mathbf{u}\} = \{\mathbf{u}^f\} + \{\mathbf{u}^s\} + \{\mathbf{u}^R\} \tag{1.1}$$

Consider the case that a foundation has two degrees of freedom in sway and rocking (x, θ) at the base of its super-structure as illustrated in **Fig. 1.1**. The interaction forces, $\{\mathbf{p}\}$ ($=\{p_x \quad p_\theta\}^T$), from the super-structure cause the inertia interaction motions, $\{\mathbf{u}^R\}$, in the frequency domain to be:

$$\begin{Bmatrix} u_x^R \\ u_\theta^R \end{Bmatrix} = \begin{bmatrix} H_{xx}(s) & H_{x\theta}(s) \\ H_{\theta x}(s) & H_{\theta\theta}(s) \end{bmatrix} \begin{Bmatrix} p_x \\ p_\theta \end{Bmatrix} \tag{1.2}$$

where,

$$\begin{bmatrix} H_{xx}(s) & H_{x\theta}(s) \\ H_{\theta x}(s) & H_{\theta\theta}(s) \end{bmatrix} = [\mathbf{H}] \tag{1.3a}$$

is the flexibility (compliance) at the top of the foundation, and

$$s = i \cdot \omega \tag{1.3b},$$

in which $i = \sqrt{-1}$, and ω is the excitement circular frequency. In the method presented in this report, the motion of a shaking table is controlled by directly following the above-described process of soil-structure interaction.

Fig. 1.2 shows a schematic view of the set-up in a shaking table test for earthquake simulation, in which a superstructure model is placed directly on the table without a physical ground model. The soil-structure interaction effects are simulated by adding appropriate soil-structure interaction motions to the free-field ground motions at the shaking table. In the simulation, first, the transducers at the base of the foundation pick up the signals of the base forces, p_x and p_θ in sway and rocking motions, respectively. These two amplified signals are then applied to the circuits H_{xx}, $H_{\theta x}$, $H_{x\theta}$ and $H_{\theta\theta}$ to produce the outputs corresponding to the soil-structure interaction motions, u_x^R and u_θ^R. The output signals are then added to the signals of the base input motions, $u_x^f + u_x^s$ and $u_\theta^f + u_\theta^s$, to produce the signals of foundation motions, $u_x^f + u_x^s + u_x^R$ and $u_\theta^f + u_\theta^s + u_\theta^R$. The method is, thus, based on the premise that

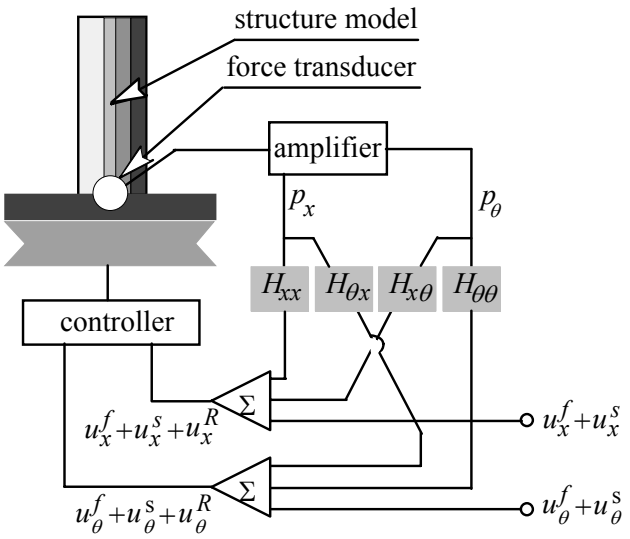

Fig. 1.2 Present setup in a shaking table test for soil-structure interaction simulation

$u_x^f + u_x^s$ and $u_\theta^f + u_\theta^s$ are known beforehand as the base input motions. The signals of the foundation motions are finally translated into the shaking table motions by the shaking table controller.

This method, therefore, requires a device that can generate signals identical to the transient motion of its base on a soil medium of infinite extent. To all intents and purposes, the expression of soil stiffness, $[\mathbf{k}]$ $(=[\mathbf{H}]^{-1})$, must be simplified enough for the device to loose no time in responding to the input force $\{\mathbf{p}\}$, and producing the soil-structure interaction motion, $\{\mathbf{u}^R\}$.

1.2 PHYSICAL INTERPRETATION OF DYNAMIC SOIL STIFFNESS

Observation of wave fronts radiating from a foundation offers important insights into soil-structure interaction. This is also a very useful way to examine simple expressions of soil-structure interaction. Konagai et al[1), 2)] used a special experiment method to directly observe the wave front radiating from a foundation subjected to an impulse. In the method, a foundation model is put on, or embedded in a soft and transparent soil model, which is made of urethane gel with a thin gelatin plate sandwiched upright in its middle. The elastic constants of the gelatin plate are more or less identical to those of the surrounding urethane gel. Since the gelatin has an extremely high photo-elastic sensitivity compared with the urethane gel, the gelatin plate allows the visual observation of the radial propagation of shear waves in the vicinity of the foundation. A vertical impulse was applied to a model of a rigid surface disk. **Fig. 1.3** shows a snap

shot of the wave front radiating outwardly into the homogeneous ground model. The hemispherical shape of the wave front suggests that the wave decays as it travels away in the radial direction, r. This wave with the velocity c is approximated by:

$$u^R = q(r) \cdot f(r - ct) \tag{1.4}$$

where, $q(r)$ describes how the wave attenuates as it travels away. On the soil-disk interface ($r = r_0$) having the contact area, A, the reaction force, p, is schematically described as:

$$\begin{aligned} p \cong \tau A = -\left\{ A\mu \frac{\partial u^R}{\partial r} \right\}_{r=r_0} &= -A\mu \left\{ \frac{dq}{dr} f + q \frac{\partial f}{\partial r} \right\} \\ &= -A\mu \left\{ \frac{dq}{dr} f - \frac{q}{c} \frac{\partial f}{\partial t} \right\}_{z=z_0} \\ &= -A\mu \left\{ \frac{q'}{q} u^R - \frac{1}{c} \dot{u}^R \right\} \end{aligned} \tag{1.5}$$

in which μ is the elastic modulus of soil.

The force p thus turns out to comprise two components proportional to the displacement, u^R, and the velocity, $\dot{u}^R$, of the disk, respectively. Equation (1.5) is thus rewritten as:

$$p = K \cdot u^R + C \cdot \dot{u}^R \tag{1.6}$$

where,

$$K = \left\{ - A\mu q'(r) / q(r) \right\}_{r=r_0} \tag{1.7a}$$

$$C = \left\{ A\mu q(z) / c \right\}_{z=z_0} \tag{1.7b}$$

Since $q(r)$ decreases as r increases, $-q'(r)$ in equation (1.7a) is a positive value, and consequently, both parameters, K and C are positive. Equation (1.6), thus, implies that the stiffness of the soil-disk system is mechanically identical to an assembly of the spring K and the damper C arranged in parallel.

A simple semi-infinite soil rod with a constant cross-section ($q(r) = q(r_0) = 1$, **Fig.**

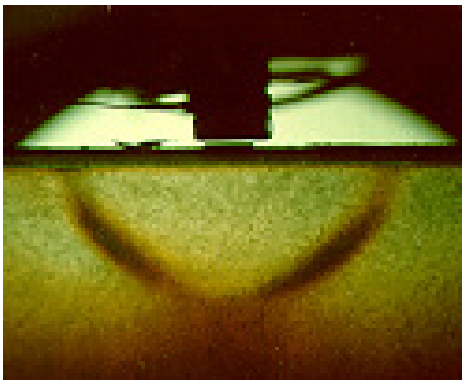

Fig. 1.3 Hemispherical wave front from a rigid disk[1), 2)]

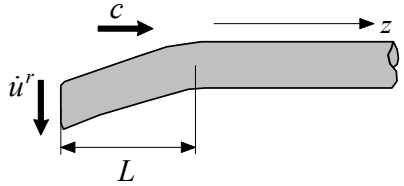

Fig. 1.4 Semi-infinite soil rod

1.4), offers further clearer physical insight into the reaction from the soil. Only shear deformation is allowed to take place in this rod. The soil stiffness at the end of the rod is simply given by:

$$k = \frac{\mu A}{L} \tag{1.8}$$

with L as the deformed length of the rod. For a static load applied to the end of the rod, the entire length of the rod is deformed ($L = \infty$), and eventually:

$$k = K = \frac{\mu A}{L} = 0 \tag{1.9a}$$

Equation (1.9a) is consistent with equation (1.7a) because $-q'(r)$ is 0 for this rod of constant cross-section. When a dynamic load p causes the rod's end to be driven with the velocity $\dot{u}^R$, the entire length of the rod does not move all at once within a limited time t. At this particular time t, displacement u^R and the deformed rod length L reach $\dot{u}^R t$ and ct, respectively. The reaction force p is thus given as:

$$p = k \cdot u^R = \frac{\mu A}{ct} \dot{u}^R t = \frac{\mu A}{c} \dot{u}^R = C \dot{u}^R \tag{1.9b}$$

It is obvious that Equation (1.9b) is consistent with equation (1.7b) because the specific energy does not decrease as the wave travels through the rod of constant cross-section calling for $q(r) = q(r_0) = 1$.

An added mass parameter, *M*, if necessary, can be attached to the simplified model for better approximation of the soil stiffness, leading to a slight modification of equation (1.6) as:

$$p = M \cdot \ddot{u}^R + K \cdot u^R + C \cdot \dot{u}^R \tag{1.10}$$

The soil stiffness is thus written in the frequency domain as:

$$k = \left(K - \omega^2 M\right) + i\omega C \tag{1.11}$$

implying that the stiffness is eventually a complex function of circular frequency ω. Its real part is a downward open parabola with its peak at $\omega = 0$, whereas its imaginary part increases linearly with increasing frequency.

1.3 SUMMARY

The above expression for the soil stiffness may be based on oversimplified conditions, but gives us an idea that the stiffness for any of lateral, vertical or rotational response mode will be approximately described by a limited number of simple frequency-independent parameters. It is, however, certainly necessary to have a rational numerical tool allowing rigorous stiffness parameters to be examined, and to be compared with the simplified expressions. Especially, thorough discussions on piles

grouped beneath super structures are essential in the course of this study; the discussion follows in ***Chapter* 2**.

REFERENCES

1) Konagai, K., Y. Koizumi and S. Ogawa,: Experiments on Soil-Pile Interaction using Electromagnetic-Induction-Type Impulse Generator, "*Dynamic Response of Pile Foundations -- Experiments, Analysis and Observation*", *Geotechnocal Special Technical Publication, ASCE*, **11**, 99-109, 1987.
2) Konagai, K. and T. Nogami: Analog circuit to simulate dynamic soil-structure interaction in shake table test, *International Journal of Soil Dynamics and Earthquake Engineering*, **17(5)**, 279-287, 1998.

Chapter 2

BEAM ANALOGY FOR SOIL-PILE GROUP INTERACTION ANALYSIS

2.1 INTRODUCTION

Piles, grouped beneath a superstructure, interact with the surrounding soil during an earthquake, and the dynamic pile-soil-pile interaction often affects the motion of the superstructure to a considerable extent. Straightforward evaluation of the pile-soil-pile interaction, however, is cumbersome especially in dealing with tens or hundreds of piles grouped together. Hence a simplified approach for the evaluation of such dynamic pile-soil-pile interaction is essential for the purpose of treating the dynamic behavior of an entire soil-foundation-structure system. A great deal of research has been carried out with the aim of developing such a simplified approach. These attempts include the Ring-Pile method (Takemiya[1)]) and Closely-Spaced-Plates model (Ohira and Tazo[2)]). In these methods, piles with the soil caught among them are re-grouped into several concentric cylinders (piles arranged in concentric circles) and soil-pile-striped upright plates, respectively, allowing close evaluation of interaction effects to be made with less time and trouble. This chapter presents a further simplified approach in which a group of piles is viewed as a single equivalent upright beam.

2.2 EQUIVALENT SINGLE UPRIGHT BEAM

2.2.1 *Superposition method for evaluation of group effect*

Prior to introducing the equivalent upright beam, straight-forward evaluation of pile-soil-pile interaction is necessary to provide rigorous solutions. Based on the numerical scheme presented by Tajimi and Shimomura[3] (Thin-Layered Method, 1976) that allows the rigorous evaluation of soil-embedded foundation interaction effects, a numerical program, *TLEM*'(Ver. 1.1), has been developed for soil-pile group interaction analysis (Konagai[4], 1998). The piles are assumed to be upright Timoshenko or Beronoulli-Euler beams embedded in a horizontally layered soil deposit with infinite extent. The evaluation of pile-soil-pile interaction effects in this program is based on the superposition method that was originally proposed by Poulos[5, 6] (1968, 1971). In this approximation, only two piles are considered in the formulation of a global flexibility matrix, and other piles' effects on these two piles are totally ignored (**Fig. 2.1**). Kanya and Kausel[7] (1982) have shown that the superposition scheme gives reasonable results not only for static loads but for dynamic loads as well.

The definition of a dynamic interaction factor $I_{i,j}$ of a pair of piles, in which a unit harmonic load ($j = x$: lateral force, $j = \phi$: moment) is applied to the first pile head (active pile) and the displacements ($i = x$: lateral sway, $i = \phi$: rocking) are evaluated for the second one (passive pile)], is as follows:

$$I_{i,j} = \frac{\textit{Dynamic displacement of passive pile}}{\textit{Static displacement of active pile}} \tag{2.1}$$

When rocking motions or moments are concerned, displacements and forces denote $r_0\phi$ and M / r_0, respectively, where r_0 is the radius of pile, ϕ is the angle of rotation of the passive pile and M is the moment applied to the head of the active pile.

Table 2.1 Parameters for piles

$E_p I_p$ (tf m^2)	ρ_p (t/m^3)	r_0 (m)	length (m)
2.4×10^5	2.0	0.5	15

Table 2.2 Parameters for surface soil deposit

ρ_p (t/m^3)	v_s (m/s)	ν	Thickness (m)
1.75	100	0.40	20

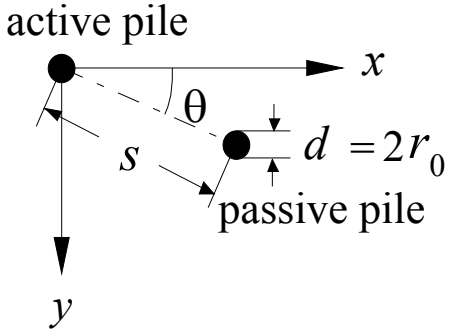

Fig. 2.1 Active and passive piles

Figs. 2.2a-2.2c show the variations of interaction factors with respect to non-dimensional frequency $\omega d / v_s$, in which ω= circular frequency, $d = 2r_0$, and v_s = shear wave velocity. The parameters used in the analyses are listed in **Tables 1** and **2**. The results are compared in these figures with the solutions by Kanya and Kausel[7] (1982). The curves calculated with *TLEM* show small spikes at the resonance frequencies of the surface soil deposit, because the bedrock underlying the surface layer is assumed to be completely rigid in *TLEM* analyses. Except for these upward spikes, the interaction factors are in good agreement with the solutions by Kanya and Kausel[7].

Given the interaction factors for all the possible pairs in a group of piles, the global flexibility matrix of the pile group is assembled. **Fig. 2.3** shows the variation of 2×2 pile-cap stiffness in *x*-direction, k_{xx}, compared with that obtained by Kanya and Kausel[7]. The good agreement between them validates *TLEM*.

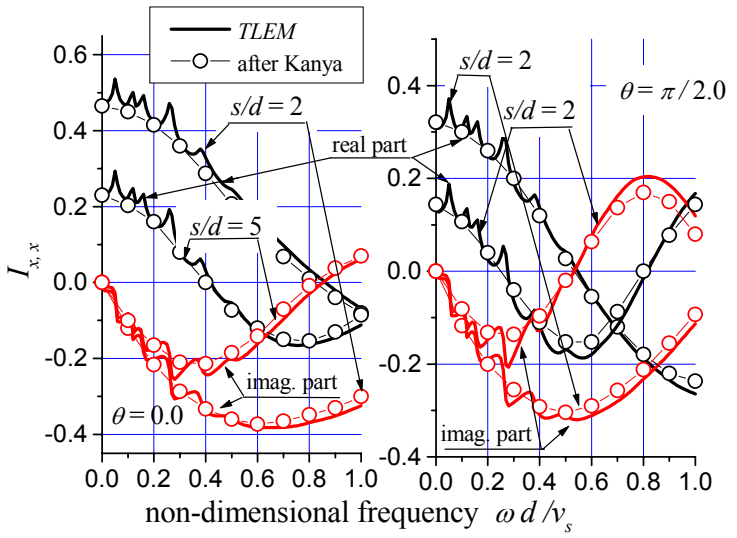

Fig. 2.2a Variations of interaction factors (I_{xx})

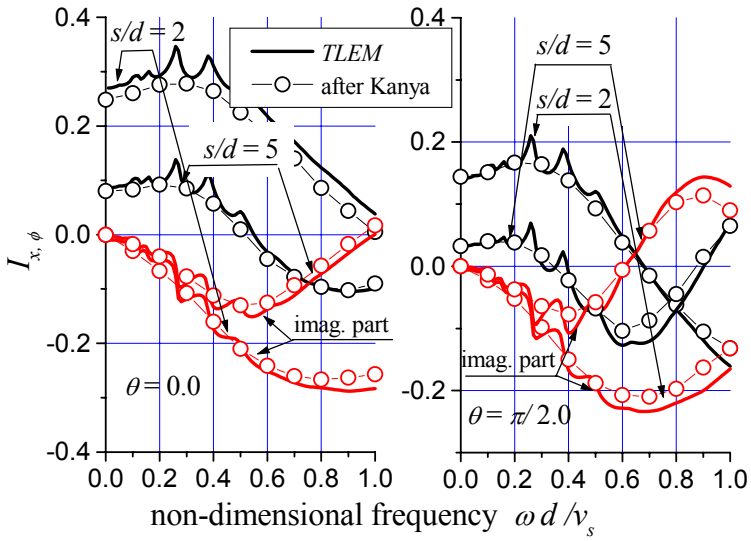

Fig. 2.2b Variations of interaction factors ($I_{x\phi}$)

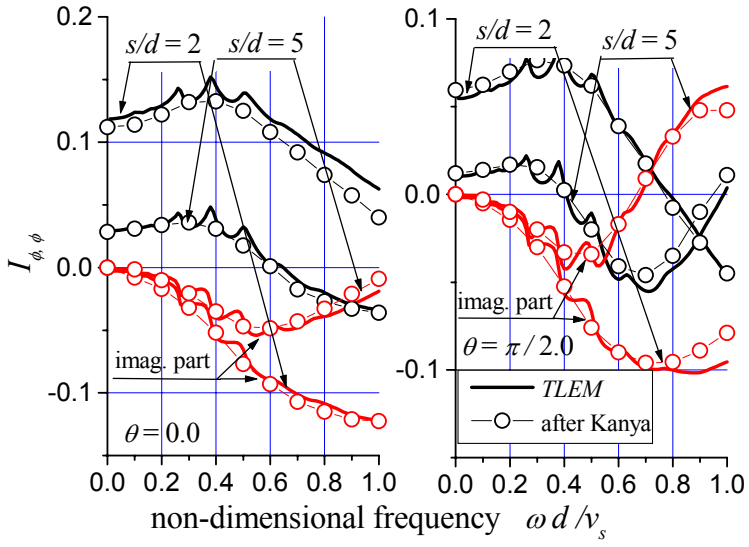

Fig. 2.2c Variations of interaction factors ($I_{\phi\phi}$)

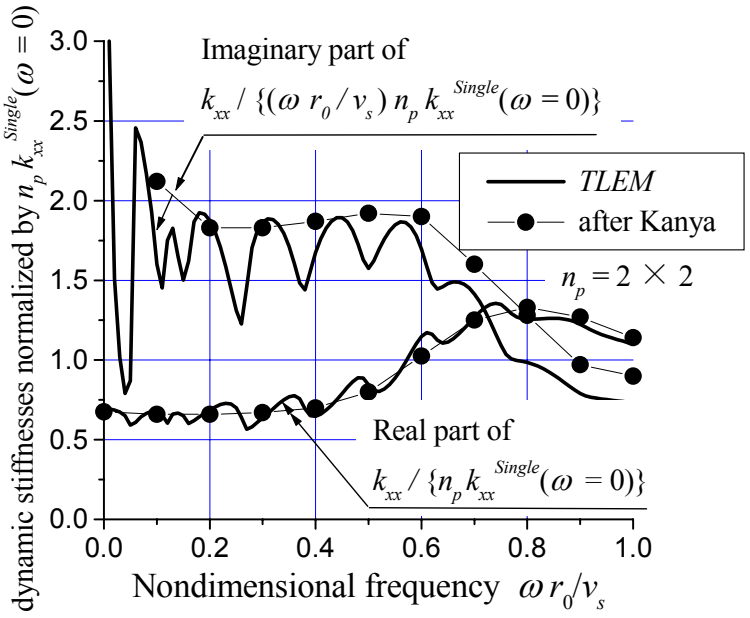

Fig. 2.3 Variations of stiffness for sway motion of 2×2 pile group

2.2.2 *Stiffness matrix of equivalent single beam*

The soil and n_p piles system is divided into n_L horizontal slices as shown in **Fig. 2.4**. The following assumptions are adopted herein to derive the stiffness matrix of the equivalent single beam:

(1) Pile elements within a horizontal soil slice are all deformed at once keeping their intervals constant, and the soil caught among piles moves in a body with the piles. The cross-section, A_g, of the equivalent single upright beam, thus, comprises both the firmly joined piles and the soil.

(2) Frictional effects due to bending of piles (external moments on each pile from soil) are ignored.

(3) Top ends of the piles are fixed to a rigid cap.

(4) All upper or lower ends of the sliced pile elements arranged on the cut-end of a soil slice remain on one plane (Note this assumption does not necessarily mean that each pile's cross-section remains in parallel with this plane. See **Fig. 2.4(b)**).

With assumptions (1), (2) and (3), lateral external forces $\{\mathbf{p}_x\}$ are described in terms of lateral displacements $\{\mathbf{u}_x\}$ and anti-symmetric vertical motion of the cap w_1 as:

$$\{\mathbf{p}_x\} = [\mathbf{L}][\mathbf{D}]^{-1}\left\{[\mathbf{L}]\{\mathbf{u}_x\} + \left\{\frac{w_1}{R_0} \quad \vdots \quad 0 \quad \cdots \quad 0\right\}^T\right\} \tag{2.2}$$

where, R_0 is the radius of the equivalent single beam, and is assumed to be identical to the radius of a circle with the same area as the cross-section A_G that includes all the

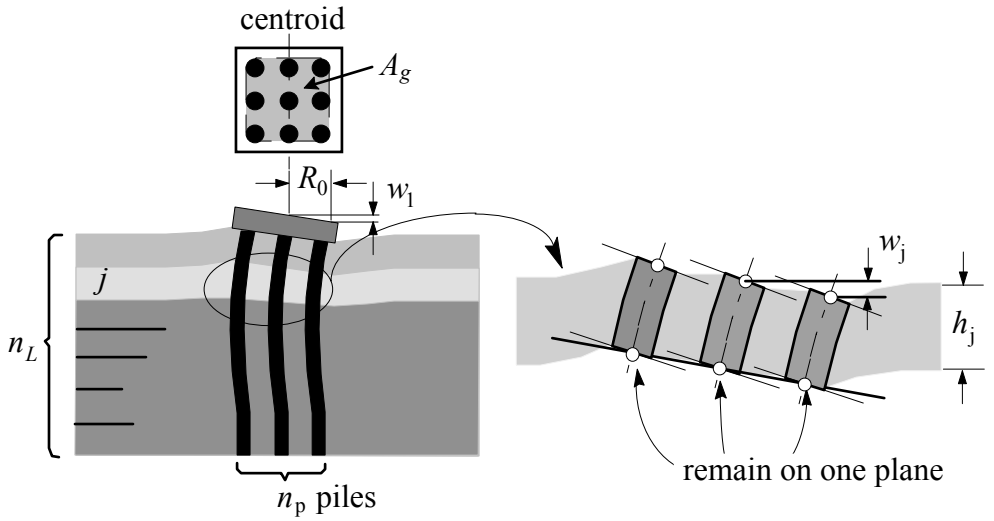

(a) soil-grouped piles system **(b)** sliced elements

Fig. 2.4 Assumptions for evaluation of equivalent single beam

grouped piles enclosed by the broken line in **Fig. 2.4a**, and

$$[\mathbf{L}]=\begin{bmatrix} -\frac{1}{h_1} & \frac{1}{h_1} & 0 & 0 & \cdots & 0 \\ \frac{1}{h_1} & -\frac{1}{h_1}-\frac{1}{h_2} & \frac{1}{h_2} & 0 & & \vdots \\ 0 & \frac{1}{h_2} & -\frac{1}{h_2}-\frac{1}{h_3} & \frac{1}{h_3} & & \vdots \\ 0 & 0 & \ddots & \ddots & \ddots & 0 \\ \vdots & & \ddots & \ddots & \ddots & \frac{1}{h_{n_L-1}} \\ 0 & \cdots & \cdots & 0 & \frac{1}{h_{n_L-1}} & -\frac{1}{h_{n_L-1}}-\frac{1}{h_{n_L}} \end{bmatrix} \tag{2.3a}$$

$$[\mathbf{D}]=\frac{1}{6}\begin{bmatrix} 2\frac{h_1}{EI_p} & \frac{h_1}{EI_p} & 0 & 0 & \cdots & 0 \\ \frac{h_1}{EI_p} & 2\left(\frac{h_1}{EI_p}+\frac{h_2}{EI_p}\right) & \frac{h_2}{EI_p} & 0 & & \vdots \\ 0 & \frac{h_2}{EI_p} & 2\left(\frac{h_2}{EI_p}+\frac{h_3}{EI_p}\right) & \frac{h_3}{EI_p} & & \vdots \\ 0 & 0 & \ddots & \ddots & \ddots & 0 \\ \vdots & & \ddots & \ddots & \ddots & \frac{h_{n_p-1}}{EI_p} \\ 0 & \cdots & \cdots & 0 & \frac{h_{n_p-1}}{EI_p} & 2\left(\frac{h_{n_p-1}}{EI_p}+\frac{h_{n_p}}{EI_p}\right) \end{bmatrix} \tag{2.3b}$$

with $EI_p = n_p \times E_p I_p$ ($E_p I_p$ = bending stiffness of a single pile).

Moment M_1 at the top ends of rigidly capped piles due to the lateral displacements $\{\mathbf{u}_x\}$ is expressed as:

$$M_1 = \left\{1st\ row\ of\ matrix\ [\mathbf{D}]^{-1}[\mathbf{L}]\right\}\{\mathbf{u}_x\}^T + D_{1,1}^{-1}\cdot\frac{w_1}{R_0} \tag{2.3c}$$

where, $D_{1,1}^{-1}$ = upper-left corner component of the matrix, $[\mathbf{D}]^{-1}$.

Assumption (4) implies that the overall anti-symmetric rocking motion of a pile group is controlled by axial motions of the piles. In other word, the external moments on the overall soil-pile system from its surrounding soil are eventually sustained by the piles that experience alternate push and pull in their axes. External moments due to the anti-symmetric vertical motions $\{\mathbf{w}\}$ are described as:

$$\left\{\frac{\mathbf{M}}{R_0}\right\}=[\mathbf{Q}]\{\mathbf{w}\} \tag{2.4}$$

where,

$$[\mathbf{Q}] = \begin{bmatrix} \frac{EI^G}{R_0^2 h_1} & -\frac{EI^G}{R_0^2 h_1} & 0 & 0 & \cdots & 0 \\ -\frac{EI^G}{R_0^2 h_1} & \frac{EI^G}{R_0^2 h_1}+\frac{EI^G}{R_0^2 h_2} & -\frac{EI^G}{R_0^2 h_2} & 0 & & \vdots \\ 0 & -\frac{EI^G}{R_0^2 h_2} & \frac{EI^G}{R_0^2 h_2}+\frac{EI^G}{R_0^2 h_3} & -\frac{EI^G}{R_0^2 h_3} & & \vdots \\ 0 & 0 & & & & 0 \\ \vdots & & & & \ddots & -\frac{EI^G}{R_0^2 h_{n_p-1}} \\ 0 & \cdots & \cdots & 0 & -\frac{EI^G}{R_0^2 h_{n_p-1}} & \frac{EI^G}{R_0^2 h_{n_p-1}}+\frac{EI^G}{R_0^2 h_{n_p}} \end{bmatrix} \quad (2.5)$$

where, EI^G is the bending stiffness of the equivalent single upright beam. This EI^G is evaluated following the same procedure as that used for the evaluation of bending stiffness of a reinforced concrete beam. Namely, EI^G is assumed to be equal to the sum of the Young's-modulus-weighted products of all the elementary areas times their distances squared from the centroid of the cross-section A_G (**Fig. 2.4a**).

Given equations (2.2)-(2.5),the global stiffness matrix of the equivalent single beam is finally expressed as:

$$\begin{Bmatrix} \mathbf{p}_x \\ \cdots \\ \dfrac{\mathbf{M}}{R_0} \end{Bmatrix} = \begin{bmatrix} [\mathbf{L}][\mathbf{D}]^{-1}[\mathbf{L}] & \vdots & \textit{1st column of } [\mathbf{L}][\mathbf{D}]^{-1} \textit{ and zeros for other columns} \\ \cdots\cdots & & \cdots\cdots \\ \textit{1st row of } [\mathbf{D}]^{-1}[\mathbf{L}] \textit{ and zeros for other rows} & \vdots & D_{1,1}^{-1} \textit{ and } [\mathbf{Q}] \end{bmatrix} \begin{Bmatrix} \mathbf{u}_x \\ \cdots \\ \mathbf{w} \end{Bmatrix} \quad (2.6)$$

TLEM has been upgraded for evaluation of the behaviors of an equivalent single beam (Ver. 1.2). **Fig. 2.5** show the variations of pile cap stiffnesses for sway motions of 2×2 and 3×3 steel pile groups (**Table 2.3**) embedded in a homogeneous soil deposit (**Table 2.4**). The curves for the equivalent single beams agree well with rigorous solutions from *TLEM* (Ver. 1.1).

Table 2.3 Parameters for steel piles

E_p (tf/m^2)	ρ_p (t/m^3)	r_0 (m)	thickness (m)	length (m)
2.1×10^7	7	0.3	0.0089	20

Table 2.4 Parameters for soil

ρ_p (t/m^3)	v_s (m/s)	ν
1.5	80	0.49

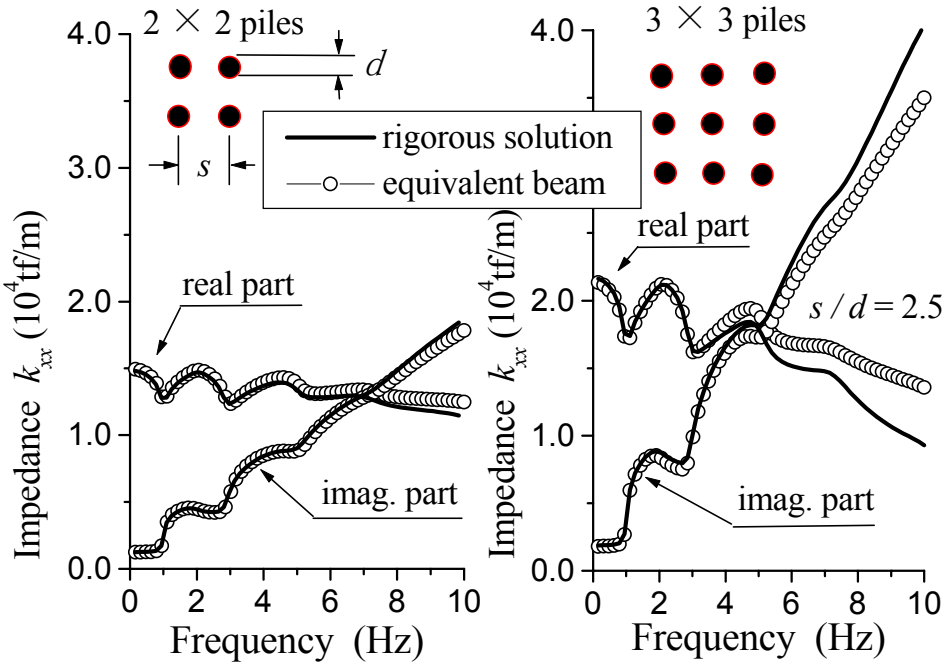

Fig. 2.5 Variations of stiffness parameters for sway motions of pile groups

The assumptions taken in this chapter to derive the stiffness matrix of the equivalent-upright beam (equation (2.6)) imply that the spacing between piles, *s*, should be within a certain limit. To investigate this constraint on the spacing between piles, the results of the program *TLEM* (Ver. 1.2) were compared with the rigorous results obtained from *TLEM* (Ver. 1.1). Here, hollow cylindrical steel piles (**Table 2.3**) embedded in a homogeneous soil (**Table 2.4**) were considered. The variations of the ratios between approximate and rigorous solutions with respect to normalized frequency $\omega s / v_s$ are shown in **Fig. 2.6** for three different values of spacing ($s/d = 2.5$, $s/d = 3.33$ and $s/d = 5.0$). For a wide range of cases examined, *TLEM* (Ver. 1.2) is found to produce insignificant error below a certain limit of spacing, $s/d < 3$. Below this limit, however, it is noted that the error can yet become significant as the

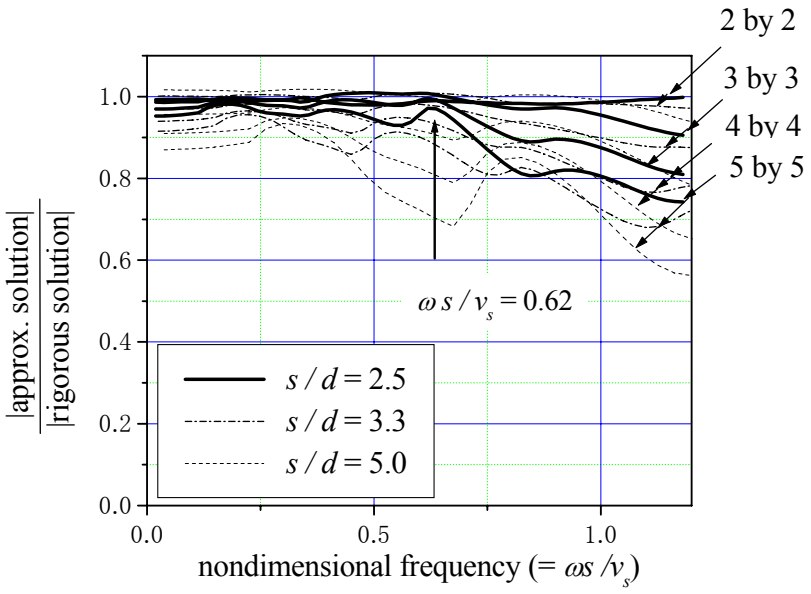

Fig. 2.6 Variation of ratios between approximate and rigorous solutions with respect to normalized frequency $\omega s / v_s$

non-dimensional frequency increases beyond a certain limit (see thick lines in **Fig. 2.6** for large number of piles).

An earthquake causes the free-field ground motion $\left\{\mathbf{u}^f\right\}$. The piles in this soil deposit, however, will not follow the free-field deformation pattern. This deviation of the displacements from the free-field soil displacements $\left\{\mathbf{u}^f\right\}$ is denoted by $\left\{\mathbf{u}^s\right\}$. Equation (2.6) is also used to evaluate effective foundation input motion $\left\{\mathbf{u}^f\right\}+\left\{\mathbf{u}^s\right\}$. The effects of soil-embedded-foundation kinematic interaction are portrayed in the form of two kinematic displacement factors in sway and rocking motions

$$T_{e,sway}=\frac{\left(u^f+u^s\right)_{sway}}{\left(u^f\right)_{sway}},\qquad T_{e,rocking}=\frac{\left(u^f+u^s\right)_{rocking}}{\left(u^f\right)_{sway}}=\frac{u^s{}_{rocking}}{u^f{}_{sway}} \qquad \text{(2.7a),(2.7b)}$$

plotted as functions of frequency. In Equation (2.7b), $u^s{}_{rocking}$ is defined as:

$$u^s{}_{rocking}=R_0\phi \qquad \text{(2.8)},$$

and it is noticed that $u^f{}_{rocking}$ is essentially identical to zero.

Fig. 2.7 shows the kinematic displacement factors of a 2×2 PC pile group ($s/d=2$, See **Tables 2.1** and 2.**2**), which are in good agreement with rigorous solutions by Fan et al.[8] (1982).

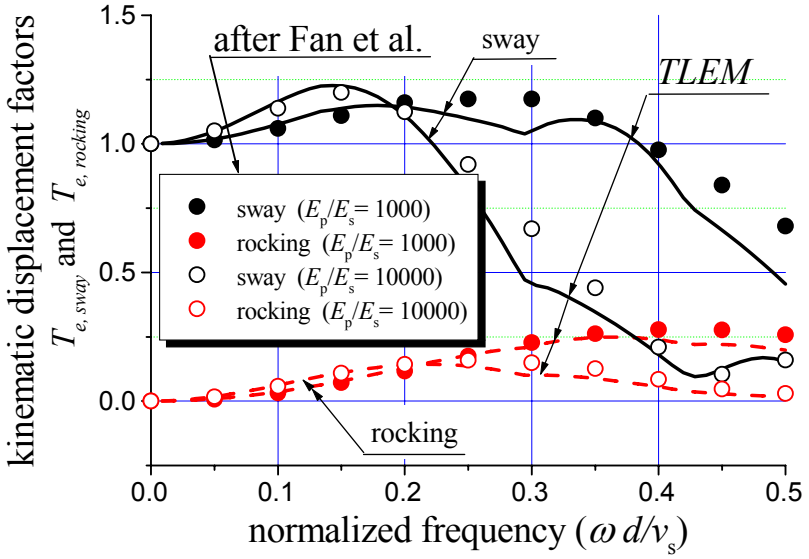

Fig. 2.7 Kinematic displacement factors of pile groups

2.3 SUMMARY

Piles grouped beneath a superstructure can be viewed as a single equivalent upright beam when the piles are closely spaced. The stiffness matrix presented herein (equation (2.6)) yields close approximations of both dynamic pile-cap stiffness and kinematic displacement factors. Given this simple beam analogy, it is shown in the following ***Chapter* 3** that salient features of soil-pile group interaction are strongly affected by their active lengths below which the piles' deflections become negligible; this fact greatly simplifies the expression of pile cap stiffness.

REFERENCES

1) Takemiya, H.: Ring-Pile Analysis for a Grouped Pile Foundation Subjected to Base Motion, *Structural Engineering/Earthquake Engineering*, *JSCE,* **3(1)**, 195s-202s, 1986.
2) Ohira, A., Tazo, T, Nakahi, S. and Shimizu, K.: Study of Dynamic Behavior of Piles in Soft Soils, *Journal of Structural Engineering / Earthquake Engineering*, 362/I-4, 417-426, 1985.
3) Tajimi, H. and Y. Shimomura: Dynamic Analysis of Soil-Structure Interaction by the Thin Layered Element Method, *Transactions of the Architechtual Institute of Japan*, **243**, 41-51, 1976.
4) Konagai, K.: Guide to *TLEM*, program manual **No. 5**, Konagai Lab., IIS, Univ. of Tokyo, 1998.
5) Poulos, H. G.: Analysis of the Settlement of Pile Groups, *Geotechnique*, **18**, 449-471, 1968.

6) Poulos, H. G.: Behavior of Laterally Loaded Piles, *Jour., Soil Mechanics and Foundation Division*, ASCE, **97(SM5)**, 733-751, 1971.
7) Kanya, A. and E. Kausel: Dynamic Stiffness and Seismic Response of Pile Groups, NSF report, **NSF/CEE-82023**, 1982.
8) Fan, K., Gazetas, G., Kanya, A., Kausel, E. and Ahmad, S.: Kinematic Seismic Response of Single Piles and Pile Groups, *Jour., Geotechnical Engineering*, ASCE, **117(12)**, 1860-1879, 1991.

Chapter 3

SIMPLE EXPRESSION OF THE DYNAMIC STIFFNESS OF GROUPED PILES

3.1 INTRODUCTION

Careful examination of deflections of grouped piles reveals that most piles are indeed flexible in practice in the sense that they do not deform over their entire lengths. Instead, pile deflections become negligible below their active lengths. With the active lengths provided for different soil-pile systems, it is shown in this chapter that pile-cap (grouped-piles-head) stiffness can be approximated in terms of mass, damping and stiffness parameters; the parameters are invariant of frequency and are dependent only on the mechanical properties of the soil and the piles. Needless to say, this study forms a part of the project to develop a new experimental method for real-time simulation of soil-structure interaction effects on shaking tables. The method requires real-time manipulation of soil-structure interaction parameters in accordance with the development of non-linear features of soils and piles. The present simple expression of pile-cap stiffness, thus, proves to be useful despite the existence of efficient numerical programs for analyzing pile-soil-pile interaction.

3.2 ACTIVE PILE LENGTH

Pile deflections become negligible below an active length L_a (**Fig. 3.1**). This length depends on how stiff the pile is in comparison with the surrounding soil. Some formulas for extreme soil profiles are certainly available (Randolf[1)], Velez[2)] and Gazetas[3)]). In

general, however, L_a is closely related to the following parameter L_0:

$$L_0 = \sqrt[4]{\frac{EI}{\mu}} \tag{3.1}$$

where, EI = bending stiffness of the pile, and μ = shear modulus of soil (representative value). The active length L_a is thus given as:

$$L_a = \alpha L_0 \tag{3.2}$$

The parameter α in the above equation differs in different soil profiles. For pile groups, EI in equation (3.1) will presumably be replaced with EI_p in equation (2.3b) in ***Chapter* 2**.

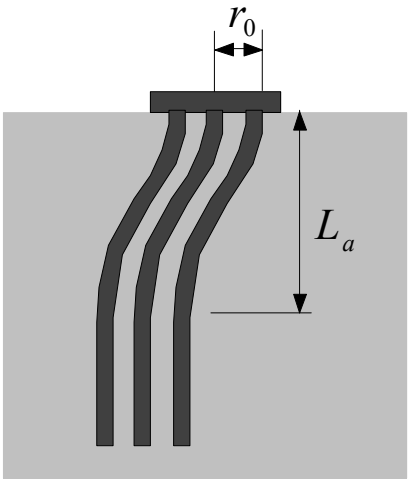

Fig. 3.1 Active length of pile

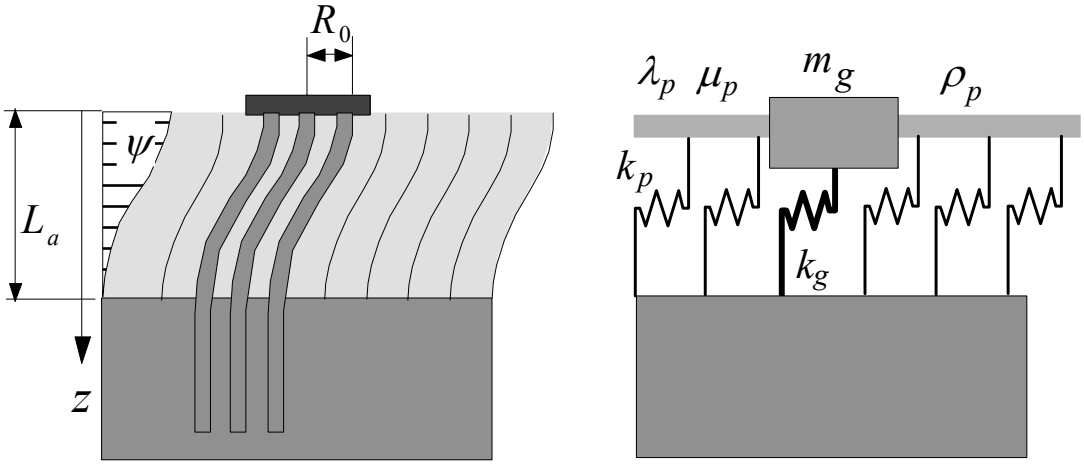

(a) Vertically sliced soil above L_a **(b)** Equivalent model

Fig. 3.2 Soil deformation

3.3 SIMPLE EXPRESSION OF PILE CAP STIFFNESS

It is assumed that only the soil above the active pile length, L_a, is deformed as shown in **Fig. 3.2a**. The upper soil is then divided into vertical soil columns. These columns, given the prescribed vibration mode ψ, can be replaced with simple-damped oscillators. Reducing the cross-section of each soil column, the soil deposit above L_a is modeled by a plane of infinite extent supported by Winkler-type springs (**Fig. 3.2b**). Lame's constants λ_p, μ_p (μ_p= shear modulus) and mass density ρ_p of the soil plane and Winkler-type spring constant k_p for the model are expressed in terms of ψ as:

$$\lambda_p = \int_0^{L_a} \lambda(z)\big(\psi(z)\big)^2 dz, \quad \mu_p = \int_0^{L_a} \mu(z)\big(\psi(z)\big)^2 dz, \quad \rho_p = \int_0^{L_a} \rho(z)\big(\psi(z)\big)^2 dz \quad \text{and}$$

$$k_p = \int_0^{L_a} \mu(z)\left(\frac{\partial\psi(z)}{\partial z}\right)^2 dz \qquad \text{(3.3a)-(3.3d)}$$

A frequency parameter, ω_0, is introduced herein as:

$$\omega_0 = \sqrt{\frac{k_p}{\rho_p}} \qquad (3.4)$$

For a homogeneous soil, parameters λ_p, μ_p and ρ_p in equations (3.3a)-(3.3c) are rewritten as

$$\lambda_p = \lambda\beta L_a, \qquad \mu_p = \mu\beta L_a \qquad \text{and} \qquad \rho_p = \rho\beta L_a \qquad \text{(3.4a)-(3.4c)}$$

Even for in-homogeneous soils too, similar expressions may be derived with λ, μ, and ρ interpreted as representative values of $\lambda(z)$, $\mu(z)$ and $\rho(z)$, and the parameter, β, portraying different soil profiles.

The expression of soil stiffness, k_s, for the lateral motion of a massless body embedded in this soil plane in **Fig. 3.2b** is completely identical to that given in Novak et al.[4] regardless of the presence of Winkler-type springs, k_p, i.e:

$$p_0 / u_0 = k_s = \pi\mu_p a_0^2 \frac{4K_1(b_0)K_1(a_0) + a_0K_1(b_0)K_0(a_0) + b_0K_0(b_0)K_1(a_0)}{b_0K_0(b_0)K_1(a_0) + a_0K_1(b_0)K_0(a_0) + b_0a_0K_0(b_0)K_0(a_0)} \qquad (3.5)$$

where, K_0 and K_1 are modified Bessel functions of the first and second order, respectively. Both a_0 and b_0 are normalized circular frequencies, and the only difference from Novak's solution, owing to the presence of Winkler-type springs, k_p, appears in a_0 and b_0 as:

$$a_0 = \frac{\omega_0 R_0}{v_T}\eta, \quad b_0 = \frac{\omega_0 R_0}{v_L}\eta \quad \text{with} \quad \eta = \sqrt{1 - \left(\frac{\omega}{\omega_0}\right)^2}$$

(3.6a)-(3.6c)

Table 3.1 Values of ξ_k and ξ_m

Poisson's ratio, ν	ξ_k	ξ_m
0.50	2.000	1.0000
0.47	1.831	0.5336
0.45	1.741	0.3740
0.43	1.667	0.2628
0.40	1.580	0.1428
0.35	1.476	0.0352
0.25	1.351	0
0.20	1.311	0
0.10	1.252	0
0.00	1.213	0

in which, ω is the circular frequency, and

$$v_T = \sqrt{\mu_p / \rho_p} \quad (= \text{transverse wave velocity in the plane}) \tag{3.6d}$$

$$v_L = \sqrt{(\lambda_p + 2\mu_p) / \rho_p} \quad (= \text{longitudinal wave velocity in the plane}) \tag{3.6e}.$$

The expression of equation (3.5) for a Poisson's ratio equal to 0.5 is obtained by taking a limit as $\nu_s \to 0.5$ in equation (3.5), i.e.:

$$k_s = 2S^* + m_s\omega^2 \tag{3.7}$$

where, $m_s (= \rho_p \pi {R_0}^2)$ is the soil mass of the same volume as the cylindrical hollow in the soil plane, and

$$S^* = 2\pi\mu \frac{a_0 K_1(a_0)}{K_0(a_0)} \tag{3.8}$$

It is found that the stiffness k_s for the Poisson's ratio other than 0.5 can be approximately expressed in the same form as equation (3.7) but with a small modification, i.e.:

$$k_s = \xi_k(\nu) \cdot S^* + \xi_m(\nu) \cdot m_s\omega^2 \tag{3.9}$$

where, ν is Poisson's ratio, and $\xi_k(\nu)$ and $\xi_m(\nu)$ are functions dependent only on a Poisson's ratio. The values $\xi_k(\nu)$ and $\xi_m(\nu)$ are given in **Table 3.1.**

Konagai et al.[5] showed that assuming plane stress condition over the entire extent of the soil plane allows k_s to approximate closely the rigorous solution of the soil stiffness, and thus, Poisson's ratio ν in equation (3.9) must be replaced with ν^* for a plane-stress medium, which is expressed as:

$$\nu^* = \frac{\lambda_p{}^*}{2(\lambda_p{}^* + \mu_p)} \tag{3.10}$$

where, $$\lambda_p{}^* = \frac{2\lambda_p \mu_p}{\lambda_p + \mu_p} \tag{3.11}$$

It is noted that ν^* ranges from 0 to 1/3, and thus, $\xi_m(\nu^*)$ in equation. (3.9) is completely equal to zero. Equation (3.9) is then rewritten as;

$$k_s = \xi_k(\nu^*) \cdot S^* \tag{3.12}$$

The function $K_1(s)/K_0(s)$ in S^* is approximated by $1 + 0.4/s$, when the absolute value of s is larger than 0.01 (Konagai et al.[6], 1998). This simplification leads to:

$$k_s = 2\pi\mu_p \xi_k(\nu^*) \frac{a_0 K_1(a_0)}{K_0(a_0)} \cong 2\pi\mu_p \xi_k(\nu^*) \cdot a_0(1 + 0.4/a_0) \tag{3.13}$$

Two limiting cases of $\omega \to 0$ and $\omega \to \infty$ are addressed herein. For the static case ($\omega \cong 0$), non-dimensional frequency a_0 is:

$$a_0 = \frac{\pi R_0}{2L_0} \tag{3.14}$$

Equation (3.13) is thus simply written as:

$$k_s \cong 2\pi\xi_k \beta\mu L_a \left(\frac{\pi R_0}{2L_a} + 0.4\right) = \mu L_a \xi_k \beta \left(\pi^2 \frac{R_0}{L_a} + 0.8\pi\right) \tag{3.15}$$

For the dynamic case ($\omega \to \infty$), non-dimensional frequency a_0 converges on:

$$a_0 = i\frac{\omega r_0}{v_T} = ia \tag{3.16}$$

Equation (3.13) is thus approximated by:

$$k_s \cong \mu L_a \xi_k \beta(i \cdot 2\pi a + 0.8\pi) \tag{3.17}$$

Form equations (3.15) and (3.17), soil stiffness will presumably be approximated as:

$$k_s \cong \mu L_a \left\{\left(\pi^2 \xi_k \beta \frac{R_0}{L_a} + 0.8\pi\xi_k \beta\right) + i \cdot 2\pi\xi_k \beta \cdot a\right\} \tag{3.18}$$

Even without the soil above the active pile length, the pile group exhibits its own stiffness, k_g (**Fig. 3.2b**), which is presumably described as:

$$k_g \cong \zeta \frac{EI_p}{L_a{}^3} = \zeta \frac{\mu L_0{}^4}{L_a{}^3} = \frac{\zeta}{\alpha^3} \mu L_0 \tag{3.19}$$

where, the value of ζ depends on the prescribed vibration mode of piles, $\psi(z)$. Both k_s and k_g sustain the mass m_g of the embedded pile group with soil caught among the piles. This mass m_g is approximated by:

$$m_g \cong \int_0^{L_a} \rho_s \pi R_0{}^2 \psi(z)^2 dz = \rho_s \pi R_0{}^2 L_a \beta \tag{3.20}$$

Therefore the overall stiffness k_{xx} of the pile cap for sway motion is given as:

$$k_{xx} = k_s + k_g - m_g\omega^2 \tag{3.21}$$

From equations (3.18), (3.19) and (3.20), equation (3.21) is rewritten as:

$$k_{xx} \cong \mu L_a\left[\left\{\pi^2\xi_k\beta\frac{R_0}{L_a} + \left(0.8\pi\xi_k\beta + \frac{\zeta}{\alpha^3}\right)\right\} + i\cdot 2\pi\xi_k\beta\cdot a - \pi\beta\cdot a^2\right] \tag{3.22}$$

Substituting equation (3.2) into equation (3.22), one obtains:

$$k_{xx} \cong \mu L_0\left[\left\{\pi^2\xi_k\beta\frac{R_0}{L_0} + \left(0.8\pi\xi_k\alpha\beta + \frac{\zeta}{\alpha^2}\right)\right\} + i\cdot 2\pi\xi_k\beta\alpha\cdot a - \pi\beta\alpha\cdot a^2\right] \tag{3.23}$$

The assumptions taken to derive the above equation may be such an oversimplification of reality that the coefficients in equation (3.23) do not always yield the best fit to the rigorous solution of k_{xx}. For more general cases, therefore, equation (3.23) will be written as:

$$k_{xx} \cong \mu L_0\left[\left\{c_1\frac{R_0}{L_0} + c_2\right\} + i\cdot c_3\cdot a - c_4\cdot a^2\right] \tag{3.24}$$

The validity of the equation (3.24) has been investigated by examining cases of different soil and pile parameters. The parameters that have been considered are pile parameters including group-pile stiffness, EI_p in Equation (2.6) (***Chapter* 2**) and active pile length ratio, L_0 / L, and soil parameters including shear modulus and material damping. In this discussion, only homogeneous soil profiles with a square arrangement of piles are considered. The best fit of the values from equation (3.24) to rigorous solutions of k_{xx} is obtained for a wide range of cases by setting c_1, c_2, c_3 and c_4 at 2π, $\pi/2$, 2π and $\pi/4$, respectively. Only some representative cases are shown in **Figs. 3.3a-3.3f**. Equation (3.24) is thus rewritten as:

$$k_{xx} \cong \mu L_0\left[\left\{2\pi\frac{R_0}{L_0} + \frac{\pi}{2}\right\} + i\cdot 2\pi\cdot a - \frac{\pi}{4}\cdot a^2\right] \tag{3.25}$$

It is noted that k_{xx} in equation (3.25) is described in terms of the following frequency-independent stiffness, damping and mass parameters, k_0, c_0 and m_0, respectively:

$$\frac{k_0}{\mu L_0} = 2\pi\frac{R_0}{L_0} + \frac{\pi}{2}, \quad \frac{c_0}{\mu L_0} = 2\pi \quad \text{and} \quad \frac{m_0}{\mu L_0} = \frac{\pi}{4} \tag{3.26a)-(3.26c}$$

The present simple expression of k_{xx} (equation (3.25)) allows the effects of overall site non-linearity to be reflected by simply replacing the shear modulus of the intact soil, μ, with the complex modulus, $\mu'(1+iD)$, that describes equivalent-linear features of the soil experiencing dynamic loading, and is obtained from shear-modulus-reduction and damping ratio curves of the soil. This manipulation, however, causes the stiffness and damping parameters, k_0 and c_0, in equations (3.26a) and (3.26b) to be slightly dependent on frequency as:

$$\frac{k_0}{\mu' L_0} = \left(2\pi \frac{R_0}{L_0} + \frac{\pi}{2} \right) - 2\pi D \cdot a \tag{3.27a}$$

$$\frac{c_0}{\mu' L_0} = 2\pi + \left(2\pi \frac{R_0}{L_0} + \frac{\pi}{2} - \frac{\pi}{4} a^2 \right) D \tag{3.27b}$$

When the effect of D cannot be ignored in equations (3.27a) and (3.27b), appropriate values of k_0 and c_0 must be determined taking into account the most probable predominant frequency a in the soil-structure interaction reality. **Figs. 3.3a-3.3b** show that introducing the complex shear modulus of soil allows the effect of material damping to be properly taken into account.

From the study of a wide range of pile parameters (viz. number of piles, diameter of individual piles and length of piles), it has been found that equation (3.25) is valid irrespective of pile and soil parameters as long as the active-pile-length ratio, L_0 / L, is within a certain limit. Beyond this limit the behavior of piles deviates from the 'flexible' nature. **Figs. 3.3c-3.3e** show this trend of the deviation of equation (3.25) from the results of "TLEM" (Ver. 1.2) as the ratio L_0 / L increases. In these figures L_0 / L is changed by the arbitrarily changing number of piles and/or diameter of individual piles. These figures show that the allowable limit of L_0 / L is about 0.4.

Equation (3.25) underestimates slightly the real part of stiffness, and overestimates its imaginary part for lower values of shear modulus of soil as can be seen in **Fig. 3.3f**. The downward dips in these non-dimensional plots of rigorous variations of k_{xx} vs. frequency occur at essentially the resonance frequencies of the soil stratum for vertical shear wave propagation. Thus the results from *TLEM* analyses with a perfectly rigid base laid under the soil stratum correspond to cases where this effect is most pronounced. It is therefore more likely that the solutions adhere along the ridges of these plots as the bases become more flexible.

There is scope to extend this study for heterogeneous soil-profile and local non-linearity of soil that develops in the vicinity of piles. In this extension also, active pile length, if rationally estimated, would allow pile-cap stiffness to be approximately described in a similar manner.

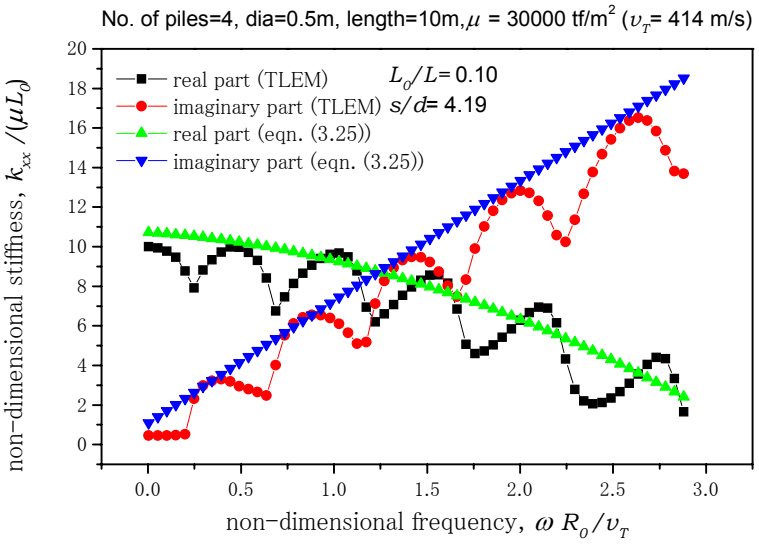

Fig. 3.3a Comparison between equation (3.25) and the results of "TLEM" (Ver. 1.2) ($D = 0.05$)

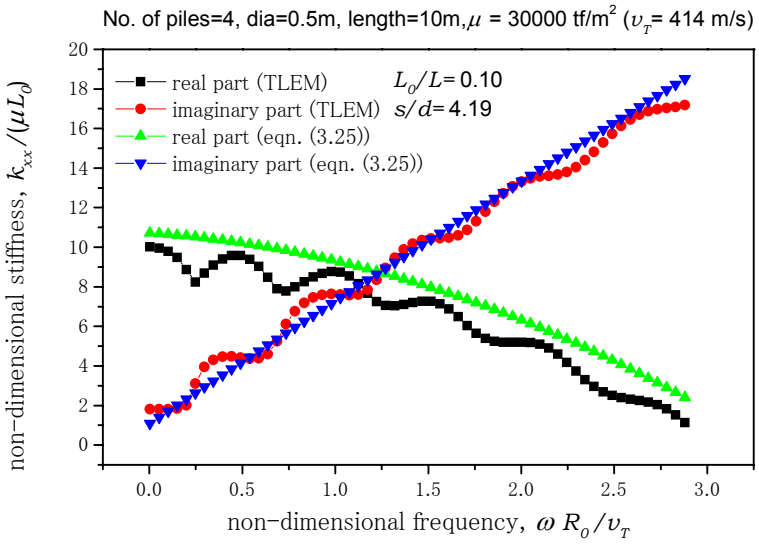

Fig. 3.3b Comparison between equation (3.25) and the results of "TLEM" (Ver. 1.2) ($D = 0.20$)

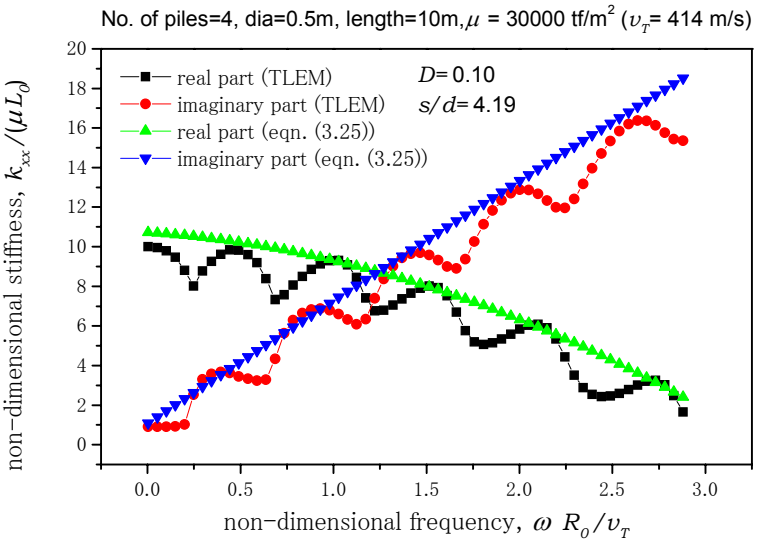

Fig. 3.3c Comparison between equation (3.25) and the results of "TLEM" (Ver. 1.2) (L_0/L = 0.10)

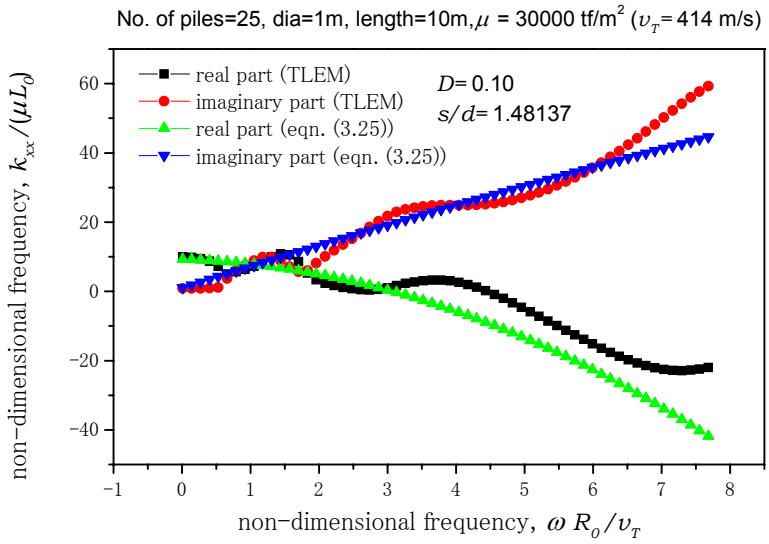

Fig. 3.3d Comparison between equation (3.25) and the results of "TLEM" (Ver. 1.2) (L_0/L = 0.31)

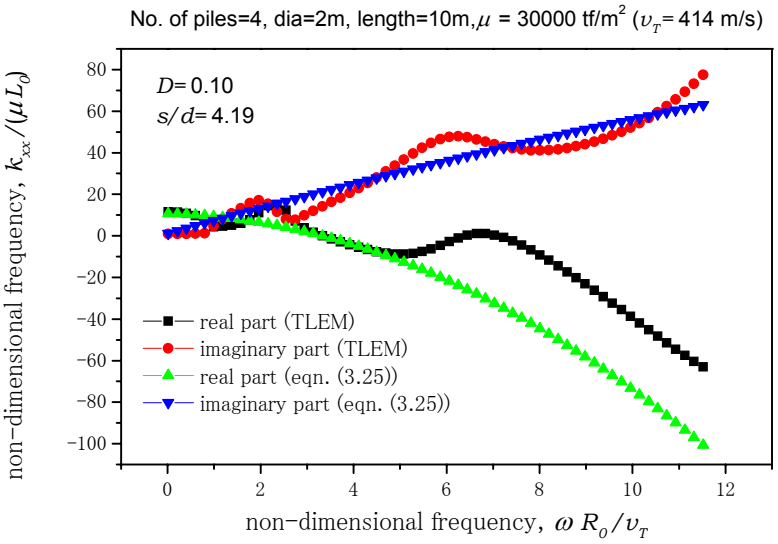

Fig. 3.3e Comparison between equation (3.25) and the results of "TLEM" (Ver. 1.2) (L_0/L = 0.40)

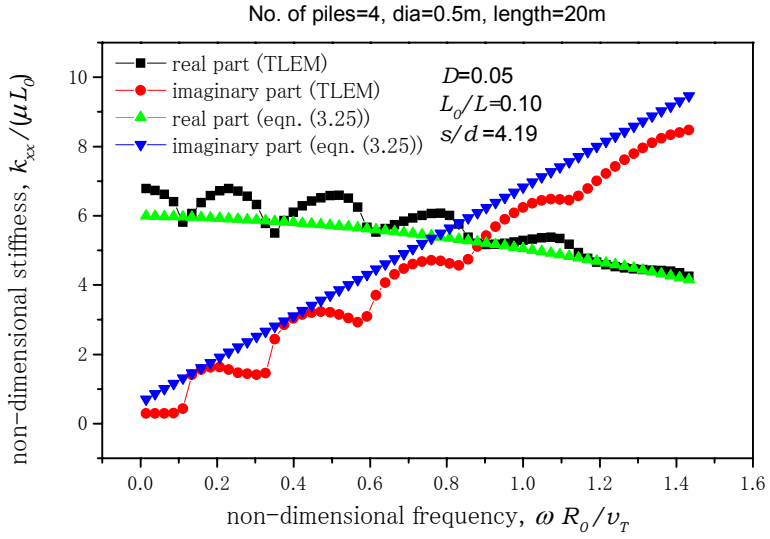

Fig. 3.3f Comparison between equation (3.25) and the results of "TLEM" (Ver. 1.2) (μ = *1875 tf/m²*, υ_T = 103.5 m/s)

3.4 SUMMARY

The idealization of grouped piles as a single equivalent upright beam (***Chapter* 2**) and the concept of the active pile length have facilitated the derivation of a simple expression of pile-cap stiffness in terms of frequency-independent mass, damping and stiffness parameters (equations (3.26a)-(3.26c)). This expression is valid irrespective of pile and soil parameters as long as the pile group exhibits "flexible" nature with its active-pile-length ratio, L_0 / L, kept less than 0.4. The present simple expression of pile-cap stiffness also allows the effects of overall site non-linearity to be reflected by simply replacing the shear modulus of the intact soil, μ, with the complex modulus, $\mu'(1+iD)$, that describe equivalent-linear features of the soil experiencing the seismic motion.

There is further scope to extend this study for heterogeneous soil-profiles and local non-linearity of soil that develops in the vicinity of piles. In this extension also, active pile length, if rationally estimated, would allow pile-cap stiffness to be approximately described in a similar manner. A similar expression might also be derived for the dynamic stiffness of grouped piles in rocking motion and for the coupled stiffness between lateral sway and rocking motions. Further detailed study on these points will be addressed in a later publication.

REFERENCES

1) Randolph, M. F.: Response of Flexible Piles to Lateral Loading, *Geotecnique*, **31(2)**, 247-259, 1981.
2) Velez, A., Gazetas, G., and Krishnan, R.: Lateral Dynamic Response of ConstrainedHead Piles, *Journal of Geotechnical Engineering*, ASCE, **109(8)**, 1983
3) Gazetas, G. and Dobry, R.: Horizontal Response of Piles in Layered Soils, *Journal of Geotechnical Engineering*, ASCE, **110(1)**, 20-40, 1984.
4) Novak, M., Nogami, T. and Aboul-Ella, F.: Dynamic Soil Reactions for Plane Strain Case, *Proc., ASCE*, 104(EM4), 953-959, 1978.
5) Konagai, K. and Maehara, M.: Study on Hypotheses for Simple Numerical Evaluation of Soil-Embedded Structure Interaction, *Bull., Earthquake Resistant Structure Research Center*, **25**, 39-60, 1992.
6) Konagai, K. and T. Nogami: Analog circuit to simulate dynamic soil-structure interaction in shake table test, *International Journal of Soil Dynamics and Earthquake Engineering*, **17(5)**, 279-287, 1998.

Chapter 4

SIMPLE EXPRESSION OF THE DYNAMIC STIFFNESS OF RIGID EMBEDDED FOUNDATIONS

4.1 INTRODUCTION

Flexible piles have been the focus of the previous discussions in ***Chapters*** **2** and **3**. The idealization of grouped piles as a single equivalent upright beam and the concept of the active pile length have facilitated the derivation of a simple expression of the pile-cap stiffness in terms of frequency-independent mass, damping and stiffness parameters. This simple approximation, however, is not appropriate for a stiff embedded body subjected to dynamic loading. Moreover, the rigidity of the foundation prevents it from following closely horizontal component of the free-field deformation pattern $\left\{\mathbf{u}^{f}\right\}$.

It is shown in this chapter that salient features of soil-stiff embedded foundation are often insensitive to the detailed variations of soil profiles, and this fact enables us to apply the method discussed in this chapter for soil-structure interaction simulation to real complex conditions. Nonlinear effects of soil will presumably be taken into account by changing the frequency-independent mass, spring and damping parameters with change in the soil shear modulus. Therefore, it is worthwhile to examine if rather secondary factors can be eliminated so that the simulations have a good balance between mathematical rigor and uncertainty in the complex environment.

4.2 KINEMATIC INTERACTION

A foundation of radius R_0 is assumed to be embedded in a soil deposit underlain by a semi-infinite bed-rock as shown in **Fig. 4.1**. The inability of the rigid embedded foundation to conform to the deformation of soil thus causes the motion of the soil-structure interface to deviate by $\{\mathbf{u}^s\}$ from the free-field motion $\{\mathbf{u}^f\}$ (kinematic interaction). The foundation input motion must thus be modified to incorporate the effect of the kinematic interaction. The foundation-input motion $\{\mathbf{u}^f\}+\{\mathbf{u}^s\}$ for the system illustrated in **Fig. 4.1** is estimated rigorously by using the thin layered element method (Tajimi and Shimomura[1)]). **Fig. 4.2** shows the variation of $\left(u^f{}_x + u^s{}_x\right)/u^f{}_x$, i.e., the foundation-input motion at the ground surface, which is normalized by the free-field motion $u^f{}_x$. The ratio is nearly a real function of frequency, and decreases gradually as the frequency increases beyond the first fundamental natural circular frequency ω_0 of the soil deposit. This implies that the contribution of the fundamental vibration mode ψ_1 of the soil deposit to the foundation-input motion is predominant, because the rigidity of the embedded foundation keeps it from following the motion of higher modes. Therefore, it might be acceptable to approximate the foundation input motion excluding the higher modes of vibration. To examine this point, the free-field motion is calculated by taking into account only the first mode of vibration ψ_1, and compared with the rigorous solution. **Fig. 4.3** shows the variation of the approximate solution of $\left(u^f{}_x + u^s{}_x\right)/u^f{}_x$. The similarity is immediately apparent when **Fig. 4.3** is compared with **Fig. 4.2**, and thus, provides a firm basis for this approximation.

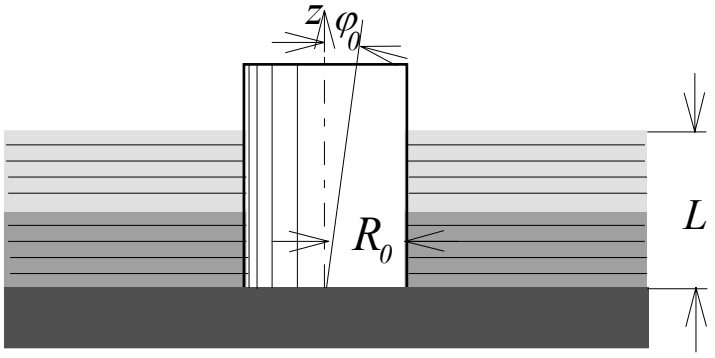

Fig . 4.1 Foundation embedded in thin-layered soil deposit

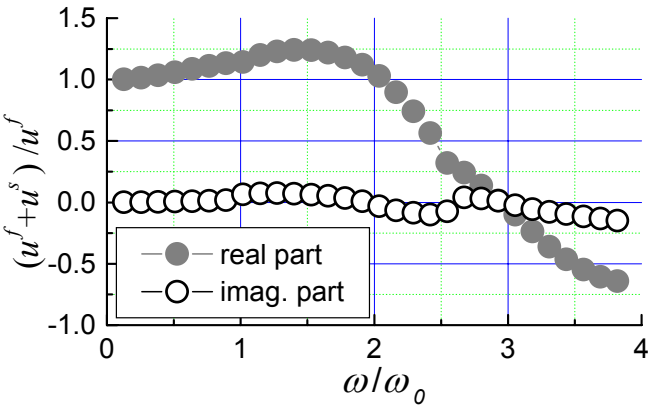

Fig. 4.2 Foundation input motion

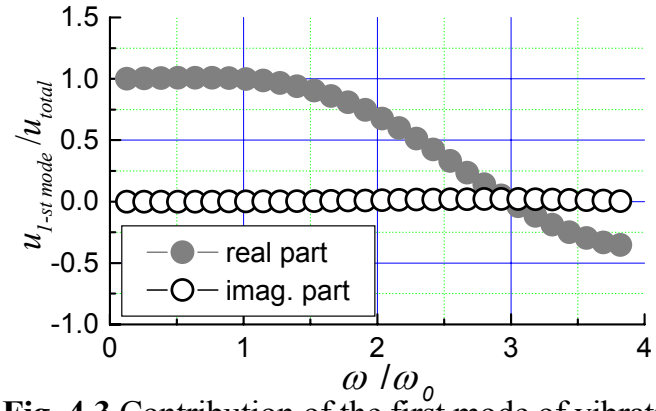

Fig. 4.3 Contribution of the first mode of vibration to free-field motion

4.3 SIDE SOIL STIFFNESS FOR ROCKING MOTION

When the embedded foundation experiences an intense earthquake motion, the surface soil deposit exhibits more pronounced nonlinear features than the bed-rock. As a result, soil shear moduli at different depths in the surface layer vary with time. On the contrary, densities and Poisson's ratios of soils are very little or negligibly influenced by the soil nonlinearity. Thus the rocking stiffness of an embedded foundation reflects the overall change in soil shear moduli throughout the depth.

The following linear variation of shear wave velocity with respect to the depth z is assumed with specific values of shear wave velocities at the top and bottom of the surface soil deposit:

$$v_T(z) = \left(v_T(L) - v_T(0)\right) \cdot \frac{z}{L} + v_T(0) \tag{4.1}$$

where, L is the thickness of the surface soil deposit. The shear wave velocities are modified to fluctuate randomly around the values given by equation (4.1) so that the

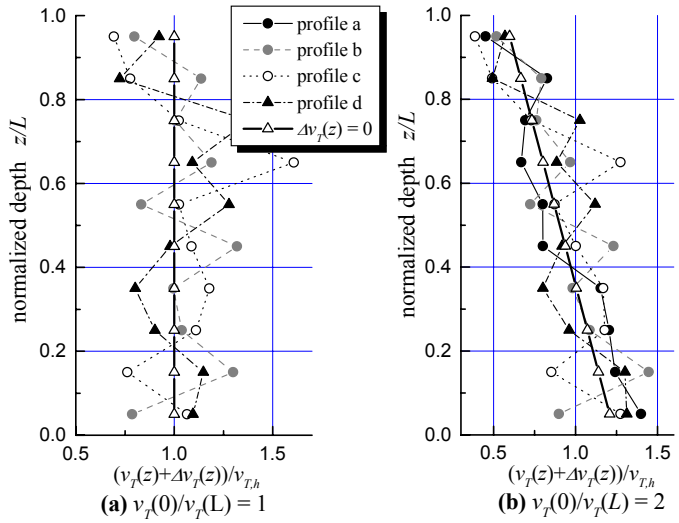

Fig. 4.4 Soil profiles (The soil deposit is divided into 10 sub-layers)

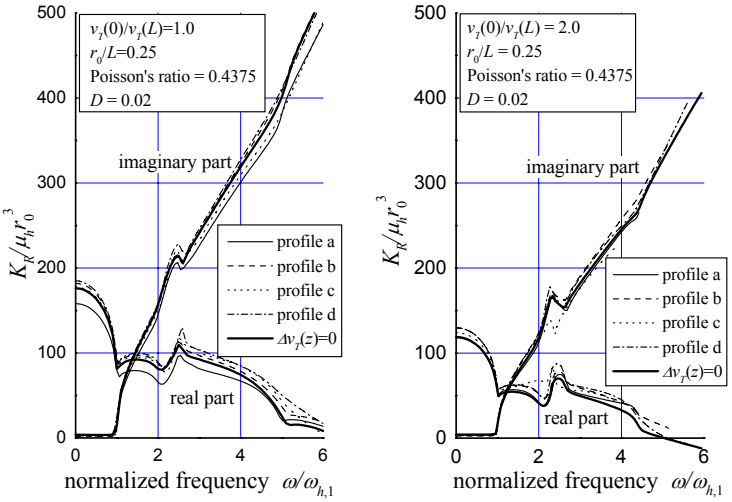

(a) $v_T(0)/v_T(H) = 1$ **(b)** $v_T(0)/v_T(H) = 2$

Fig. 4.5 Impedance functions for rocking motion of an embedded body

ratio of the deviation $\Delta v_T(z)$ to $v_T(z)$ eventually exhibits the Gaussian distribution with the standard deviation of 20%. Finally, the obtained shear wave velocities at various depths are multiplied by a uniform factor throughout the depth, to keep the fundamental resonance frequency equal to that for the original simple soil profile described by equation (4.1). Following this procedure, four different soil profiles are prepared for each of two different cases of $v_T(0)/v_T(L)=1$ and $v_T(0)/v_T(L)=2$ as shown in **Fig. 4.4a** and **4.4b**. Impedance functions for the rocking mode of the embedded foundation were computed for these soil profiles by using Thin-Layered Element Method.

Figs. 4.5a and **4.5b** show the computed rocking stiffnesses (impedance functions). It is noted that the change in the soil profile to the extent shown in **Figs. 4.4a** and **4.4b** causes no serious change in the stiffness of the foundation. These examples suggest that the rocking stiffness of a stiff embedded foundation is strongly governed by the fundamental natural frequency of the surrounding soil deposit, and rather secondary detailed features can be eliminated. It is therefore worth examining the contribution of the first fundamental vibration mode of the soil deposit to the impedance function of the foundation.

The present simulation approach utilizes simple expressions for soil responses at the side of the embedded foundation, which are obtained neglecting the vertical soil response for the horizontal and rocking responses of the foundation. This assumption was first used by Tajimi[2] (1969). Modified Tajimi's solution shows that the restoring moment M_r for the harmonic rotation $\varphi_0 e^{i\omega t}$ is expressed in the form of:

$$M_r = k_{R,side}\varphi_0 e^{i\omega t} \tag{4.2}$$

where,

$$k_{R,side} = \frac{8\mu r_0^{\,3}}{\pi}\frac{L}{r_0}\sum_{m=1,3,5..}^{\infty}\frac{\zeta_m^{\,2}\Omega_m}{m^4}$$

$$\Omega_m = \frac{4K_1(b_m)\cdot K_1(a_m) + a_m K_1(b_m)K_0(a_m) + b_m K_1(a_m)K_0(b_m)}{a_m K_0(a_m)K_1(b_m) + b_m K_0(b_m)K_1(a_m) + a_m b_m K_0(a_m)K_0(b_m)}$$

$$a_m = \zeta_m\frac{\omega_1 r_0}{v_T},\quad b_m = \zeta_m\frac{\omega_1 r_0}{v_L^*},\quad \omega_1 = 2\pi f_1 = \frac{\pi v_T}{2L}$$

$$\zeta_m = \sqrt{m^2(1+iD) - \left(\frac{\omega}{\omega_1}\right)^2} \tag{4.3a)-(4.3f)}$$

where K_m is modified Bessel function of order m. Though the original Tajimi's solution is based on the assumption of vanishing vertical displacement, the modified longitudinal wave velocity v_L* is used here to consider the stress free condition on the ground surface (Konagai and Maehara[3], 1992). The contribution of the first

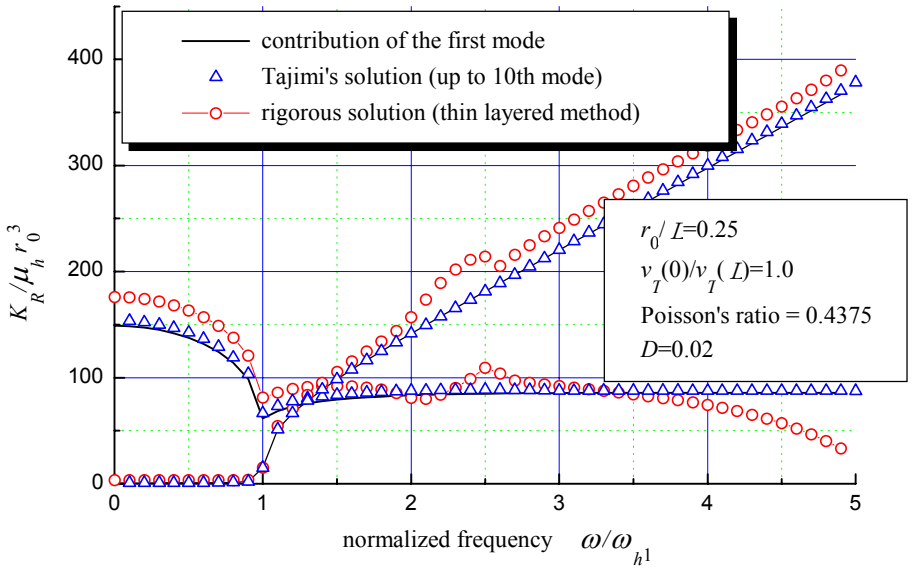

Fig. 4.6 Contribution of the first vibration mode of surrounding soil to impedance function

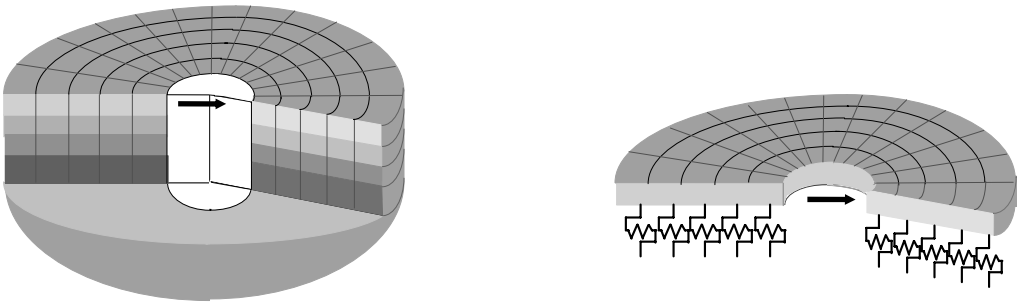

(a) soil deposit surrounding an embedded body (b) soil plane overlying Winkler springs

Fig. 4.7 Vertically sliced soil deposit

mode is isolated from the other modes in this expression. The impedances computed in this manner is compared in **Figure 4.6** to those computed with up to 10 modes. They are also computed by the thin-layered element method which does not ignore the vertical soil response and is considered to be rigorous compared with Tajimi's method. It is clear in this figure that the exclusion of higher vibration modes in Tajimi's method affects little the dynamic stiffness, and the good agreement between the rigorous and approximate solutions proves the predominant contribution of the fundamental vibration mode.

All the examples mentioned above shows that salient features of the impedance

function of a stiff embedded foundation are insensitive to the detailed variations of soil profiles and, thus, this allows us to describe the impedance function by only a limited number of parameters.

The superior contribution of the fundamental vibration mode ψ_1 to soil-embedded rigid body interaction greatly simplifies the soil-embedded body interaction analysis. When the surface soil deposit is divided into vertical soil columns as shown in **Fig. 4.7a**, these columns, given a prescribed vibration mode of ψ_1, can be replaced with simple-damped oscillators. Reducing the size of each soil column, the surface layer is modeled by a plane of infinite extent supported by Winkler-type springs (**Fig. 4.7b**). The similarity is immediately apparent when **Fig. 4.7** is compared with **Fig. 3.2** in ***Chapter* 3**, and it is now obvious that the rocking stiffness, K_R, of the embedded foundation has the same form as k_s in equation (3.15) (***Chapter* 2**), with L^2 added to its right-hand side as:

$$K_R = L^2 \cdot \xi_k(\nu^*) \cdot S^* \tag{4.4}$$

Further extended discussion on the stiffness could be made in the similar manner as that in ***Chapter* 3**. In ***Chapter* 3**, downward dips in the plots of rigorous variations of k_{xx} vs. frequency were ignored in discussing simplified expression of k_{xx} in terms of the frequency-independent mass, spring and damping parameters. **Figs. 4.5** and **4.6**, however, show that these dips are rather clearer and more significant than those appeared in k_{xx} of flexible pile groups. Substituting equations (3.6a) and (3.6c) in equation (4.4) yields both the real and the imaginary parts of K_R as

$$\frac{\mathrm{Re}(K_R)}{2\pi\mu_p\xi_k(\nu^*)} = \begin{cases} a_0 + 0.4 & \cdots \quad \omega < \omega_0 \\ 0.4 & \cdots \quad \omega > \omega_0 \end{cases} \tag{4.5a}$$

$$\frac{\mathrm{Im}(K_R)}{2\pi\mu_p\xi_k(\nu^*)} = \begin{cases} 0 & \cdots \quad \omega < \omega_0 \\ a_0 & \cdots \quad \omega > \omega_0 \end{cases} \tag{4.5b}$$

Noting that $a_0 = \omega_0 R_0 / v_T = (\pi/2)\cdot(R_0/L)$ at $\omega = 0$, the real part of K_R drops from $0.4 + (\pi/2)\cdot(R_0/L)$ down to 0.4 as ω approaches ω_0. The drop thus depends on the aspect ratio R_0/L of the foundation. For thick and short foundation, this drop is remarkable and cannot be ignored.

The stiffness S^* in equation (4.4) or its inverse, namely, a flexibility function $H^*(=1/S^*)$ is the most frequently encountered expression in soil-structure interaction analyses. The flexibility function H^* is found to be closely approximated by the following form as:

$$H^*(\omega) = A_e \frac{1}{i\omega + \alpha_e} + A_c \frac{\omega_0}{(i\omega + \alpha_c)^2 + \omega_0^2} \tag{4.6}$$

where, $A_e = A_c \cdot \left(\frac{2L}{R_0} - 1 \right)$, $A_c = 0.44 - 004 \cdot \log_2 \frac{L}{R_0}$

$\alpha_e = \left(1.2 + 0.4 \cdot \log_2 \frac{L}{R_0} \right) \cdot \omega_0$, $\alpha_c = \left(0.21 - 0.01 \cdot \log_2 \frac{L}{R_0} \right) \cdot \omega_0$ and

$\omega_0 = \frac{\pi v_s}{2L}$

(4.7a)-(4.7e)

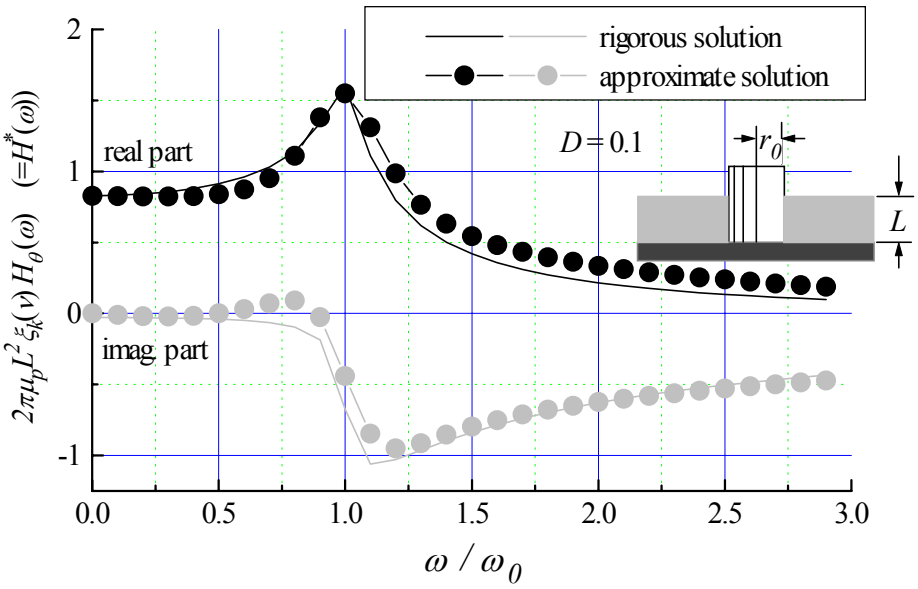

(b) Height-radius ratio (=L / r_0)) = 2.0

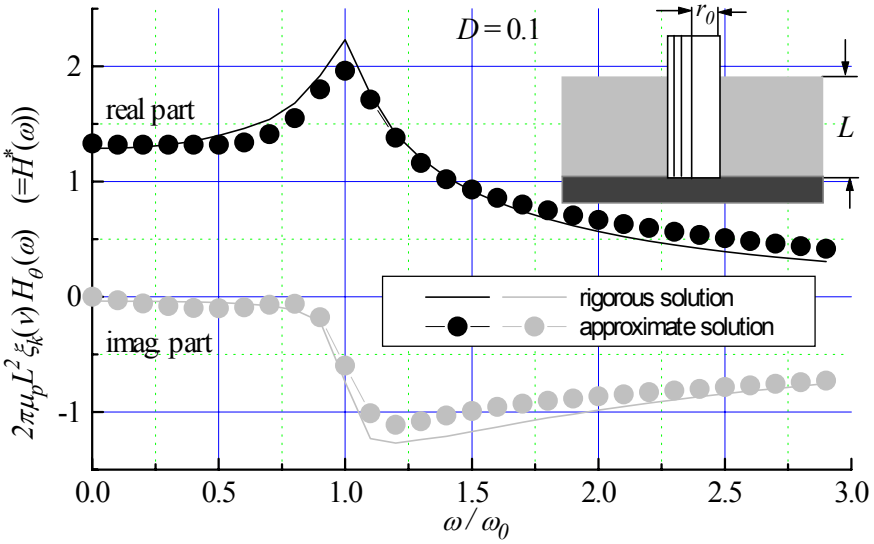

(c) Height-radius ratio $(L/r_0) = 4.0$

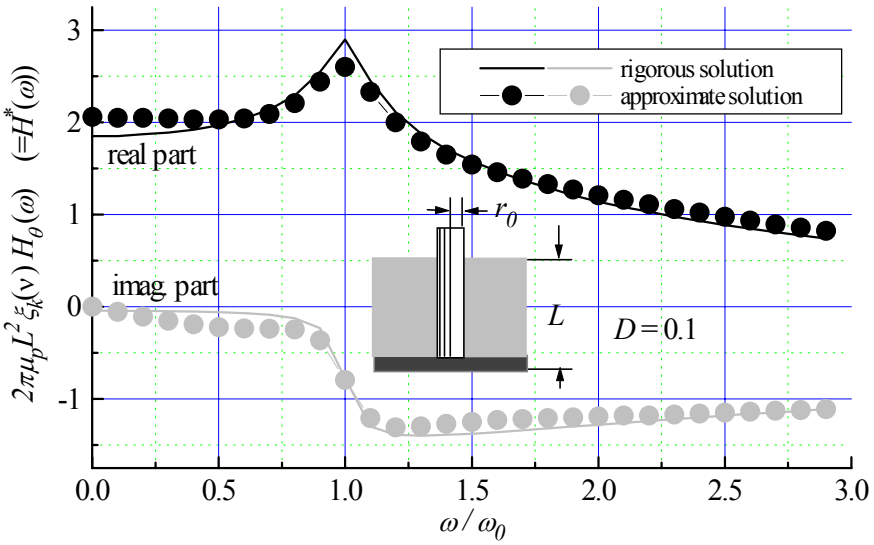

(d) height-radius ratio $(=L/r_0) = 8.0$

Fig. 4.8 Flexibility functions $H^*(\omega)$ for different height-radius ratios

Figs. 4.8a-4.8c show flexibility functions for the rocking motion of an embedded rigid cylinder for different height-radius ratios (L/R_0), 2, 4 and 8, respectively. Within this

range of radius-height ratio, the expression agrees well with the rigorous solution. Inverse Fourier transformation of H^* yields the impulse response function $h^*(t)$ as:

$$h^*(t) = A_e h_e(t) + A_c h_c(t) \tag{4.8}$$

where, $h_e = e^{-\alpha_e t}$, $h_c = e^{-\alpha_c t}\cos\omega_0 t$ (4.9a), (4.9b)

Equation (4.8) implies that the impulse response function, $h^*(t)$, is approximated by adding up exponential and exponentially decaying cosine functions.

4.4 SIMPLE EXPRESSION OF STIFFNESS

Needless to say, use of the simple models that have been discussed so far leads to some loss of precision, to be sure, however, reviewing these expressions, it is found that the impulse responses of these models are closely approximated by summing up exponential and/or exponentially decaying sine and cosine functions of time t, $h_{e,m}(t)$, $h_{c,m}(t)$ and $h_{s,m}(t)$, namely,

$$h(t) = \sum_{m=1}^{n} (A_{e,m} h_{e,m}(t) + A_{c,m} h_{c,m}(t) + A_{s,m} h_{s,m}(t)) \tag{4.10}$$

where, $A_{e,m}$, $A_{c,m}$ and $A_{s,m}$ are unknown constants and

$$h_{e,m}, h_{c,m}(t), h_{s,m}(t) = \begin{cases} e^{-\alpha^{e,m}t}, \quad e^{-\alpha_{c,m}t}\cos\omega_{c,m}t, \quad e^{-\alpha_{s,m}t}\sin\omega_{s,m}t & t \geq 0 \\ 0 & t < 0 \end{cases} \tag{4.11}$$

Fourier transforms of $h_{e,m}(t)$, $h_{c,m}(t)$ and $h_{s,m}(t)$ in equation (4) are:

$$\mathcal{F}(h_{e,m}(t)) = H_{e,m}(s) = \frac{1}{s+\alpha_{e,m}} = \frac{s+\alpha_{e,m}}{s^2 + 2\alpha_{e,m}s + \alpha_{e,m}{}^2} \tag{4.12a}$$

$$\mathcal{F}(h_{c,m}(t)) = H_{c,m}(s) = \frac{s+\alpha_{c,m}}{s^2 + 2\alpha_{c,m}s + \alpha_{e,m}{}^2 + \omega_{c,m}{}^2} \tag{4.12b}$$

$$\text{and} \quad \mathcal{F}(h_{s,m}(t)) = H_{s,m}(s) = \frac{\omega_{s,m}}{s^2 + 2\alpha_{s,m}s + \alpha_{e,m}{}^2 + \omega_{s,m}{}^2} \tag{4.12c}$$

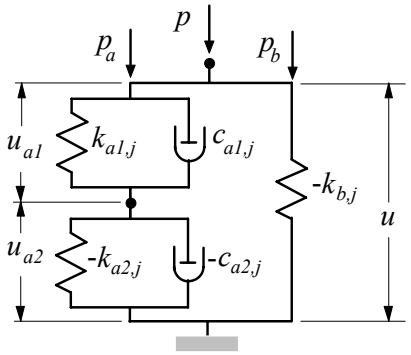

Fig. 4.9 Mechanical model for basic response functions

where, $s = i\omega$ and $\mathcal{F}$ denotes Fourier transformation.

It is noted here that the flexibility function of an assembly of three springs, k_{a1}, k_{a2}, k_b, and two dashpots, c_{a1}, c_{a2}, shown in **Fig. 4.9**[4] is expressed in the following form as:

$$H(s) = \frac{(c_{a2} + c_{a1})s + (k_{a2} + k_{a1})}{c_{a1}c_{a2}s^2 + \{k_{a1}c_{a2} + k_{a2}c_{a1} + k_b(c_{a2} + c_{a1})\}s + k_{a1}k_{a2} + k_b(k_{a2} + k_{aj})} \quad (4.13)$$

which has the same form as any of equations (4.12a), (4.12b) and (4.12c). Setting $c_{a1}c_{a2}$ in equation (4.13) at a minus constant value -1, for example, and equating all the terms in equation (4.13) with those of equation (4.12a), five model parameters, k_{a1}, k_{a2}, k_b, c_{a1} and c_{a2} are given as real values as:

$$k_{a1} = 0.618\alpha_{e,m} \quad (4.14a)$$

$$k_{a2} = -1.618\alpha_{e,m} \quad (4.14b)$$

$$k_b = 0 \quad (4.14c)$$

$$c_{a1} = 0.618 \quad (4.14d)$$

$$c_{a2} = -1.618 \quad (4.14e)$$

It is noted here that the mechanical model with the above five parameters (equations (4.14a)-(4.14e)) is identical to a simple Kelvin-Voigt model with a single spring, $-\alpha_{e,m}$, and a single dashpot, -1, arranged in parallel. Similarly, the parameters for equation (4.12b) are obtained as:

$$k_{a1} = (0.618\alpha_{c,m} + \omega_{c,m}) \quad (4.15a)$$

$$k_{a2} = -(1.618\alpha_{c,m} + \omega_{c,m}) \quad (4.15b)$$

$$k_b = -2.236\omega_{c,m} \quad (4.15c)$$

$$c_{a1} = 0.618 \quad (4.15d)$$

$$c_{a2} = -1.618 \quad (4.15e)$$

and those for equation (4.12c) are:

$$k_{a1} = \alpha_{s,m} - \frac{\omega_{s,m}}{2}$$

(4.16a)

$$k_{a2} = -\alpha_{s,m} - \frac{\omega_{s,m}}{2} \tag{4.16b}$$

$$k_b = 1.25\omega_{s,m} \tag{4.16c}$$

$$c_{a1} = 1 \tag{4.16d}$$

$$c_{a2} = -1 \tag{4.16e}$$

Needless to say, springs and dashpots should be positive in actuality. If these parameters were free from this restriction however, it would surely be possible for equation (4.13) to be completely identical to any of equations (4.12a), (4.12b) and (4.12c), and this assumption is possible in both analog circuits and digital signal processors as is demonstrated later in ***Chapter* 5**.

The side soil stiffness, K_R (equation (4.4)), for the rocking motion of an embedded rigid body is, thus, approximated by a simple mechanical model illustrated in **Fig. 4.10**.

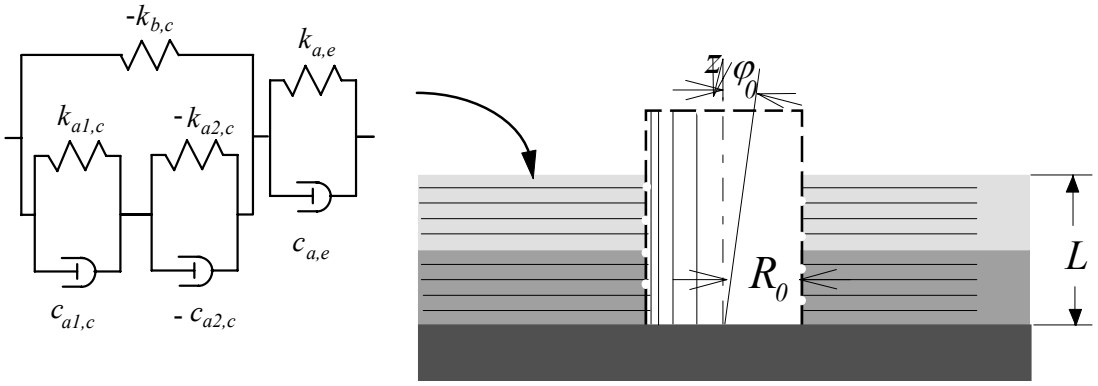

4.5 BASE SOIL STIFFNESS

Fig. 4.10 Simple expression of side soil stiffness

Differing from flexible pile foundations, the contribution of a base reaction to the stiffness of an embedded rigid body is not always small enough to be ignored. Unit-impulse functions of soil/rock, at the base of a rigid embedded foundation, are assumed to be those for a half-space medium. According to the approach presented by Meek and Wolf[5)-9)] (1992-1993), the soil is idealized as a truncated semi-infinite elastic cone with its own apex height z_0 (**Fig. 4.11**), in order to develop unit-impulse functions for a surface foundation. The apex ratio z_0 / r_0, or the opening angle of the cone, is determined for each degree of freedom such that the static stiffness coefficient of the disk on the cone is equal to that on the semi-infinite soil half-space. It is noted that, although the cone is defined for the static condition, wave propagation through the cone dominates the behavior in the high frequency range. For a translational motion, the unit-impulse response function $h_x(t)$ is thus obtained as:

$$h_x(t) = \begin{cases} \dfrac{1}{K_{x,static}} \dfrac{v_T}{z_0} e^{-\frac{v_T}{z_0}t} & t > 0 \\ 0 & t < 0 \end{cases} \tag{4.17}$$

with $K_{x,static} = \rho {v_T}^2 \cdot \pi {r_0}^2 / z_0$, where v_T is the shear wave velocity. The unit-impulse response function $h_\theta(t)$ for a rotational response is similarly obtained as:

$$h_\theta(t) = \begin{cases} \dfrac{1}{K_{\theta,static}} \dfrac{{v_L}^*}{z_0} e^{-\frac{3{v_L}^*}{2 z_0}t} \left(3\cos\dfrac{\sqrt{3}}{2}\dfrac{{v_L}^*}{z_0}t - \sqrt{3}\sin\dfrac{\sqrt{3}}{2}\dfrac{{v_L}^*}{z_0}t \right) & t > 0 \\ 0 & t < 0 \end{cases} \tag{4.18}$$

with $K_{\theta,static} = 3\rho {v_L}^2 I_0 / z_0$, where $I_0 = (\pi/4) {r_0}^4$ and ${v_L}^*$ is the modified longitudinal wave velocity (Meek and Wolf[5)-9)]).

The above expressions for unit-impulse functions are also found to be linear combinations of exponential and/or exponentially decaying sin and cosine functions.

4.6 SUMMARY

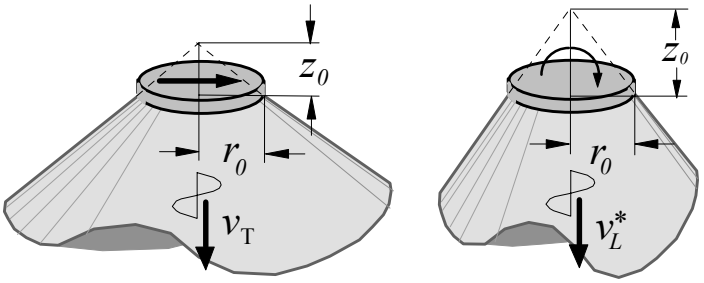

Fig. 4.11 Cones for various degrees of freedom (Meek and Wolf[5)-9)])

Salient interaction features are often insensitive to the detailed variations of soil profiles. As for an embedded stiff foundation, its impedance function (stiffness) is strongly governed by the fundamental vibration mode of the surrounding soil deposit and the contributions by other modes can be ignored. This fact allows us to describe the impedance function by only a limited number of parameters. Such a small number of parameters are easily manageable even in commercially-available personal computers. This simplification thus certainly enhances the practicality of the present simulation approach and also will enable us to use the present simulation approach in the nonlinear soil environment.

REFERENCES

1) Tajimi, H. and Y., Shimomura: Dynamic analysis of soil-structure interaction by the thin layered element method, *Proc., Architectural Institute of Japan*, **243**, 41-51. 1976.
2) Tajimi, H.: Dynamic analysis of a structure embedded in an elastic stratum, *Proc. 4th World Conf.*, *Earthquake Engineering*, Santiago, Chile, **III**(**A-6**), 53-69, 1969.
3) Konagai, K. and M., Maehara, M.: Study on hypotheses for simple numerical evaluation of soil-embedded structure interaction, *Bull., Earthquake Resistant Structure Research Center*, **25**, 39-60, 1992.
4) Konagai, K. and T. Nogami: Analog circuit to simulate dynamic soil-structure interaction in shake table test, *International Journal of Soil Dynamics and Earthquake Engineering*, **17(5)**, 279-287, 1998.
5) Meek, J. W. and Wolf, J. P.: Cone models for homogeneous soil, *J. geotechnical eng., ASCE*, **118(5)**, 667-685, 1992.
6) Meek, J. W. and Wolf, J. P.: Cone models for soil layer on rigid rock, *J. geotechnical eng., ASCE*, **118(5)**, 686-703, 1992.
7) Meek, J. W. and Wolf, J. P.: Cone models for embedded foundation, *J. geotechnical eng., ASCE*, **120(1)**, 60-80, 1992c.
8) Meek, J. W. and Wolf, J. P.: Cone models for nearly incompressible soil, *Earthquake eng. struct. Dyn.,* **22**, 649-663, 1993.
9) Meek, J. W. and Wolf, J. P.: Why cone models can represent the elastic half space, *Earthquake eng. struct. Dyn.,* **22**, 759-771, 1993.

Chapter 5

REAL TIME CONTROL OF SHAKING TABLE FOR SOIL-STRUCTURE INTERACTION SIMULATION

5.1. INTRODUCTION

Simple descriptions of foundation stiffness parameters have been discussed in the first half of this report (***Chapters* 1-4**). The stiffness parameters are eventually approximated by a limited number of frequency-independent parameters. All these expressions may be such an oversimplification of reality that they cannot cover all cases of soil-structure interaction reality. They, however, allow the real-time production of the soil-structure interaction motions on a shaking table. A faithful reproduction of input motions on a shaking table, however, is not easily done when the table is heavily loaded with a structure model to be tested. This chapter presents the method for simulating soil-structure interaction effects in shaking table tests, in addition to some pieces of equipment contrived for better control of shaking tables. Simple examples of soil-structure interaction simulations are also given in this chapter.

5.2 REPRODUCTION OF SOIL-STRUCTURE INTERACTION MOTIONS

Fig. 5.1 shows a schematic view of the set-up in a shaking table test for earthquake simulation[1)-4)], in which a superstructure model is placed directly on the table without a physical ground model. The soil-structure interaction effects are simulated by adding appropriate soil-structure interaction motions to the free-field ground motions at the shaking table. In the simulation, first, the transducers at the base of the foundation pick

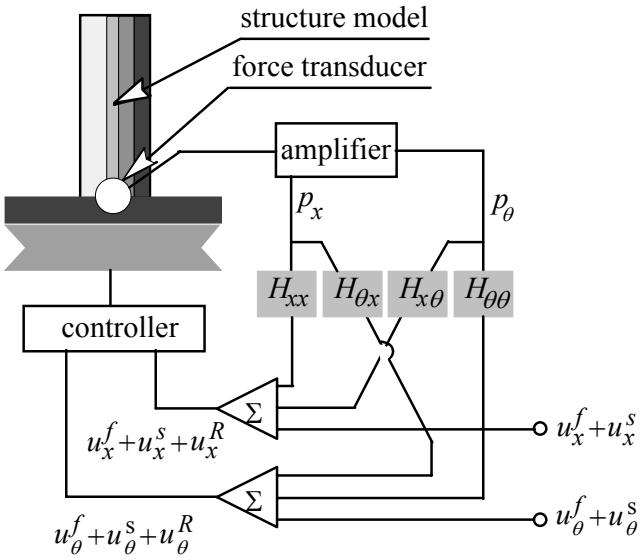

Fig. 5.1 Present setup in a shaking table test for soil-structure interaction simulation

up the signals of the base forces, p_x and p_θ in sway and rocking motions, respectively. These two amplified signals are then applied to the circuits H_{xx}, $H_{\theta x}$, $H_{x\theta}$ and $H_{\theta\theta}$ to produce the outputs corresponding to the soil-structure interaction motions, u_x^R and u_θ^R. The output signals are then added to the signals of the base input motions, $u_x^f + u_x^s$ and $u_\theta^f + u_\theta^s$, to produce the signals of foundation motions, $u_x^f + u_x^s + u_x^R$ and $u_\theta^f + u_\theta^s + u_\theta^R$. The method is, thus, based on the premise that $u_x^f + u_x^s$ and $u_\theta^f + u_\theta^s$ are known beforehand as the base input motions. The signals of the foundation motions are finally translated into the shaking table motions by the shaking table controller.

This method, therefore, requires a device that can generate signals identical to the transient motion of its base on a soil medium of infinite extent. Foundation stiffness parameters that have been discussed in the first half of this report (***Chapters* 1-4**) are found to be approximated by a limited number of frequency-independent parameters.. Reviewing these expressions as well as those by a number of researchers, it is found that they are closely approximated by summing up exponential and/or exponentially decaying sine and cosine functions of time *t*, the functions being easily produced by simple analog circuits and/or digital signal processors, namely,

$$h(t) = \sum_0^n A_j h_j(t) \tag{5.1}$$

where, A_j are unknown constants, and

$$h_j(t) = e^{-\alpha_j t} \cos(\omega_j t - \phi_j) \tag{5.2}$$

with α_j^{-1} = time constant, ω_j = circular frequency that can be zero, and ϕ_j = phase lag. Applying the Laplace transform to equation (5.2) leads to:

$$H_j(s) = \frac{(s+\alpha_j)\cdot\cos\phi_j + \omega_j \cdot \sin\phi_j}{(s+\alpha_j)^2 + \omega_j{}^2} \tag{5.3}$$

From equation (5.3), it is found that the Laplace transform of equation (5.1) eventually has a rational form that is described as:

$$H(s) = \frac{a_m s^m + a_{m-1}s^{m-1} + \cdots + a_1 s + H(0)}{b_m s^m + b_{m-1}s^{m-1} + \cdots + b_1 s + 1} \tag{5.4}$$

where, a_j and b_j ($j = 1, 2, \cdots, m$) are unknown constants, and $m \le 2n$. The constant, a_m, must be zero as far as the Laplace transforms, $H_j(s)$, (equation (5.3)) for different values of *j* are added up. However, the constant, a_m, is intentionally left in equation (5.4) for a more general expansion of the present method. Equation (5.4) is rewritten as:

$$\{\mathbf{S}\}\{\mathbf{a}\} = H(0) - H(s) \tag{5.5}$$

where,

$$\{\mathbf{S}\} = \{-s^m \quad \cdots \quad -s \quad s^m H(s) \quad \cdots \quad sH(s)\}, \tag{5.6a}$$

and

$$\{\mathbf{a}\} = \{a_m \quad \cdots \quad a_1 \quad b_m \quad \cdots \quad b_1\}^T \tag{5.6b}$$

The 2*m* unknown constants included in the coefficient vector $\{\mathbf{a}\}$ are determined in such a way that $\{\mathbf{a}\}$ allows the approximate expression of $H(s)$ described in equation (5.4) to best-fit its rigorous values in a desired frequency range. Since equation (5.6) should be satisfied for both its real and imaginary parts, *m* values of *s* are first taken within this frequency range. Then, *m* pairs of equation (5.5) (real and imaginary parts) at these particular points of *s* eventually make up a set of 2*m* simultaneous equations, and solving the linear simultaneous equations, one obtains all the coefficients in $\{\mathbf{a}\}$.

It will be worthwhile examining how closely the expression in equation (5.4) approximates rigorous solutions of flexibilities. **Fig. 5.2** shows the variation of flexibility, H_{xx}, at the cap of a 3×3 pile group (Kanya and Kausel[5]) with respect to the dimensionless frequency, a_0 ($= 2r_0\omega / v_s = 2r_0 s / iv_s$). The parameters, r_0 and v_s, are the radius of pile and the shear wave velocity in the surrounding soil, respectively. There are two numerical examples of simulation shown in this figure; one with the number of unknown constants 2*m* set at 4 ($a_0 =$ 0.3 and 0.6), another with 2*m* = 8 ($a_0 =$ 0.2, 0.4, 0.6 and 0.8). The larger the number of coefficients is, the more closely the approximate expression fits the rigorous values. It is, however, noted in this figure that even a small number of coefficients (2*m* = 4) eventually allow the close approximation to be realized over almost the entire extent of the frequency range

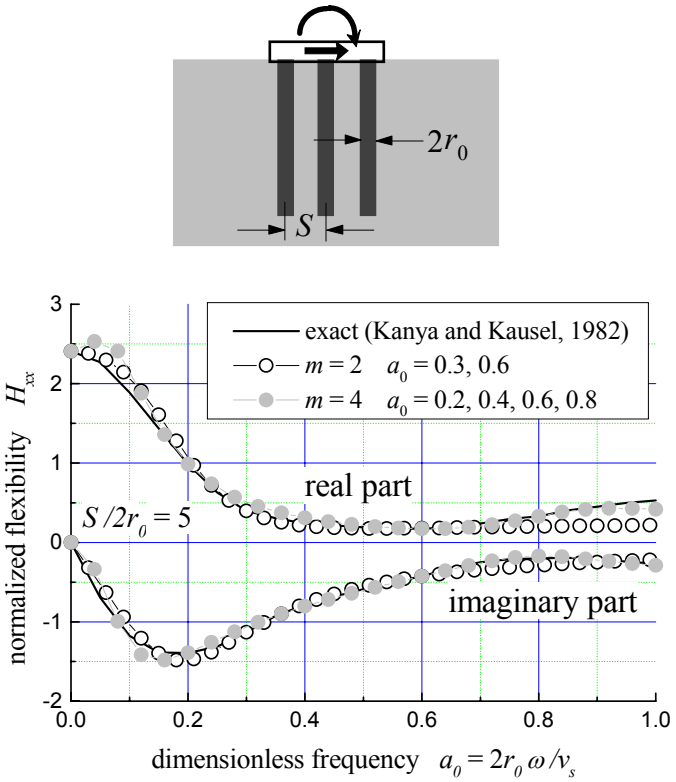

Fig. 5.2 Dynamic flexibility of 3×3 pile group for harmonic loading

($0 \le a_0 \le 1$) in this figure. The number of coefficients for approximation should be reduced to some allowable minimum. Meek and Wolf[6), 7)] have developed approximate expressions of flexibility functions for vertical, sway and rocking motions of a rigid mat foundation (radius $=r_0$) on a homogeneous half-space. Their expressions are interpreted in such a way that the allowable minimum of the number of coefficients is eight ($2m = 8$) in order for a close approximation to be obtained within the frequency range, $0 \le a_0 \le 5$. As for an embedded rigid foundation, Konagai and Nogami[3), 4)] have demonstrated that the same number of coefficients allow the flexibility function to be closely approximated for its rocking motion within the same frequency range. Simple descriptions of stiffness parameters of grouped piles are given in ***Chapter* 3**.

5.3. PRESENT SYSTEM

5.3.1 *Equivalent analog circuits*

Electric signals can be controlled by using analog circuits. The first-level units in

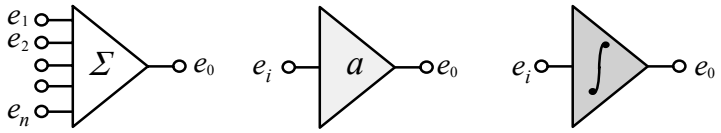

(a) adder **(b)** linear amplifier **(c)** integrator

Fig. 5.3 Key circuits

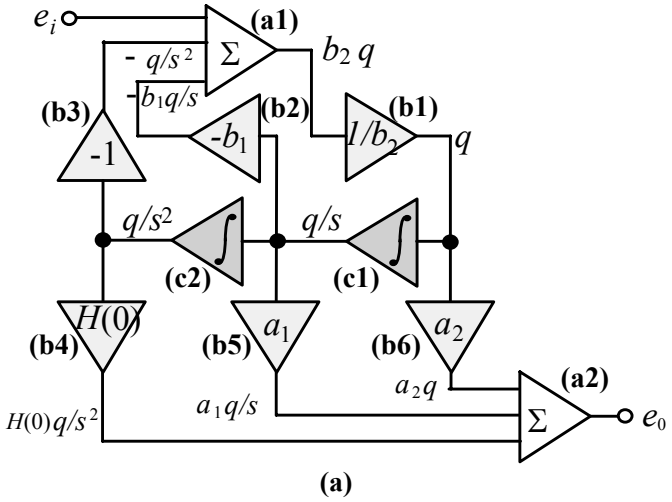

(a)

(b)

Fig. 5.4 Analog circuit to generate

the circuits are operational amplifiers and passive elements (resisters and capacitors).[8] These units form an adder (**Fig. 5.3a**), an amplifier (**Fig. 5.3b**) and an integrator (**Fig. 5.3c**) which add several different input signals ($e_1, e_2, \cdots e_n$) together, multiply an input signal, e_i, by a scale factor, *a,* and integrate a signal, e_i, respectively. The functions of both the adder and the amplifier can actually be realized by one sole circuit called a "scaled adder". For the sake of simple explanations, however, they are separately shown in **Figs. 5.3a** and **5.3b**.

(a) $e^{-\alpha_m t}$ **(b)** $e^{-\alpha_m t}\cos\omega_m t$ **(c)** $e^{-\alpha_m t}\sin 2\omega_m t$

Fig. 5.5 Basic response functions generated by the present analog circuit (0.1 s/div.)

Setting the number *m* at 2 in equation (5.4), for example, the input and output signals, e_i and e_o, of the circuit for producing the interaction motion u^r should satisfy:

$$H(s) = \frac{a_0 + a_1 s + a_2 s^2}{b_0 + b_1 s + b_2 s^2} = \frac{e_o}{e_i} \tag{5.7}$$

Introducing an unknown quantity *q*, the above equation (5.7) can be separated into the following two equations as:

$$e_o = a_0 \frac{q}{s^2} + a_1 \frac{q}{s} + a_2 q \tag{5.8a}$$

$$e_i = b_0 \frac{q}{s^2} + b_1 \frac{q}{s} + b_2 q \tag{5.8b}$$

With the expression in equations (5.8a) and (5.8b), the circuit that is capable of generating e_o to an arbitrary input signal e_i is designed as shown in **Fig. 5.4a**. The input signal e_i and two additional signals, which will be shown later identical to $-q/s^2$ and $-b_1 \cdot q/s$, are added together first by the adder **(a1)** and then multiplied by $1/b_2$ by the linear amplifier **(b1)**. The output signal in the above process is q according to equation (5.8b). Noting that integrating a signal is equivalent, in the frequency domain, to dividing its Fourier spectrum by *s*, integrators **(c1)** and **(c2)** produce signals q/s and q/s^2, respectively. After these two signals go through linear amplifiers **(b2)** and **(b3)** with scale factors $-b_1$ and -1 respectively, they become $-b_1 \cdot q/s$ and $-q/s^2$, and return to the adder **(a1)**: whereas linear amplifiers **(b4)**, **(b5)** and **(b6)** produce $H(0)\cdot q/s^2$, $a_1 q/s$ and $a_2 q$ respectively, which are added together by the adder **(a2)**. It is now clear from equation (5.8a) that the output of the adder **(a2)** is identical to the signal e_o.

Fig. 5.4b shows a model for a test try of **Fig. 5.4a**-equivalent circuit. Five pairs of knobs are for tuning the five scale factors in **Fig. 5.4a**. In **Figs. 5.5a-5.5c** examples are shown for the transient response of the circuit ($\alpha_j = 5.5\ \text{s}^{-1}$, $\omega_j = 15.7\ \text{s}^{-1}$) to an

impulse (rectangular pulse of 5V, duration time = 10 ms). Only tuning the parameters to prescribed values allows any of the basic response functions to be generated.

5.3.2 *Controller of shaking table*

It is noted that the system illustrated in **Fig. 5.1** is realized on condition that a shaking table loses no time in producing faithfully its input motion, $\{\mathbf{u}\}$ $(=\{\mathbf{u}^f\}+\{\mathbf{u}^s\}+\{\mathbf{u}^r\})$. The motion produced by the shaking table, however, is not exactly identical to the intended time history because the ratio of output-to-input amplitude of the shaking table system does not remain the same over the desired frequency range. The performance of the system's transfer function is also affected by the presence of models on the shaking table; this fact may cause the motion of the table to further deviate from the intended time history. A controller with the transfer function T normally performs like a low pass filter, and experiments on the table are conducted below its cut-off frequency. Below this frequency yet, there remains a time delay Δt between the produced motion and the input signal. The effect of the time delay, described in the frequency domain as $T \cong e^{-i\omega\Delta t}$, could be canceled by multiplying the flexibility function H by T^{-1}. Assuming that the performance of a soil-foundation system is approximated by that of a simple-damped oscillator with a spring *K*, a dashpot *C* and a mass *M* (**Fig. 5.6**), the flexibility function H_{xx} is expressed as:

$$H_{xx} = \frac{1}{K - \omega^2 M + i\omega C} \tag{5.9}$$

Thus, the cancellation of the time-delay effects is made by

$$H_{xx}T^{-1} \cong \frac{e^{i\omega\Delta t}}{K - \omega^2 M + i\omega C} \tag{5.10a}$$

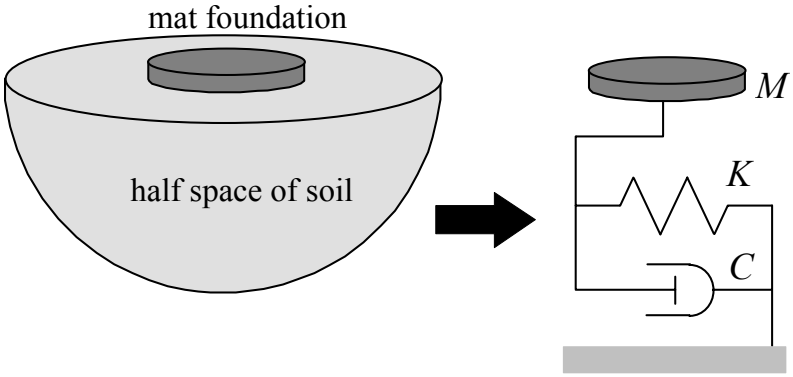

Fig. 5.6 Equivalent spring-damper system supporting a rigid mat foundation

For smaller values of $\omega\Delta t$, equation (5.10a) is rewritten as:

$$H_{xx}T^{-1} \cong \frac{1}{K-\omega^2(M-\Delta M)+i\omega(C-\Delta C)} \tag{5.10b}$$

where,

$$\Delta M = C\cdot\Delta t \tag{5.11a}$$

$$\Delta C = M\cdot\Delta t \tag{5.11b}$$

Equation (5.10b) shows that the equivalent mass and the viscous damping coefficient are reduced by $C\Delta t$ and $M\cdot\Delta t$, respectively. The reduced mass $M-\Delta M$ and the damping coefficient $C-\Delta C$ must be positive, calling for:

$$\frac{\Delta M}{M} = 4\pi^2\,\frac{t_c\Delta t}{{t_0}^2} < 1 \tag{5.12a}$$

$$\frac{\Delta C}{C} = \frac{\Delta t}{t_c} < 1 \tag{5.12b}$$

with

$$t_c = C\,/\,K \tag{5.13a}$$

$$t_0 = 2\pi\sqrt{M\,/\,K} \tag{5.13b}$$

The above conditions (equations (5.12a) and (5.12b)) are usually satisfied in reality for many cases of soil-structure interaction, because radiation of waves from a foundation leads the motion of the structure to be noticeably damped.

It is, however, necessary for the time delay to be minimized when equations (5.12a) and (5.12b) are not satisfied. One possible measure for reducing the time delay is to increase the feedback gain of a servo-amplifier of the shaking table (**Fig. 5.7**). In **Fig. 5.7**, u_{in} and u_{out} are the input signal and the signal of the motion produced by the shaking table, respectively. The deviation of the produced motion from the input signal, $u_{out}-u_{in}$, is multiplied by a negative factor $-\beta$, and is added to the input signal u_{in}. The following relationship between u_{in} and u_{out} is then satisfied with the original transfer function of the controller itself ($\beta=0$) denoted by G:

$$u_{out} = G(u_{in} + \beta(u_{in} - u_{out})) \tag{5.14}$$

From equation (5.14), the overall transfer function T is described as:

$$T = \frac{u_{out}}{u_{in}} = \frac{G+G\beta}{1+G\beta} \tag{5.15}$$

It is noted in equation (5.15) that T comes closer to 1 as the feedback gain, β, increases. The servo-amplifier shown in **Fig. 5.7** was built in a one-dimensional shaking table system to check its performance. **Fig. 5.8** shows that a servo-amplifier with a larger value of β offers more significant improvement in expanding the frequency range in which the ratio of output-to-input amplitude remains almost constant with little

phase-shift. The increase of β, however, leads to a decrease in the margin for unstable clattering of the table that is caused by the noise echoing through the closed circuit of the servo-amplifier.

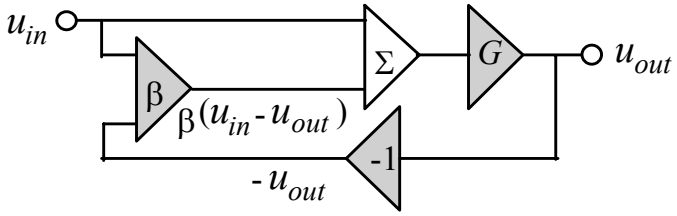

Fig. 5.7 Servo-amplifier

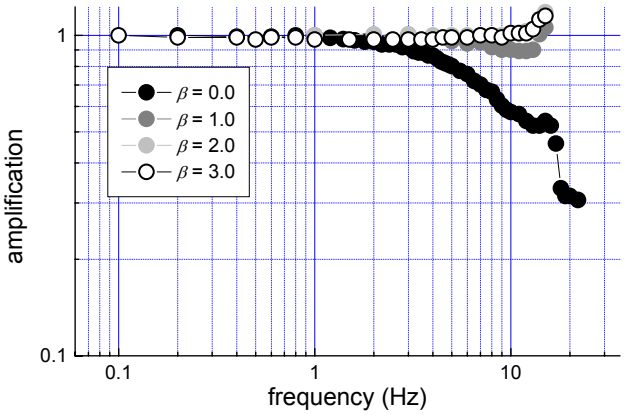

(a) amplitude

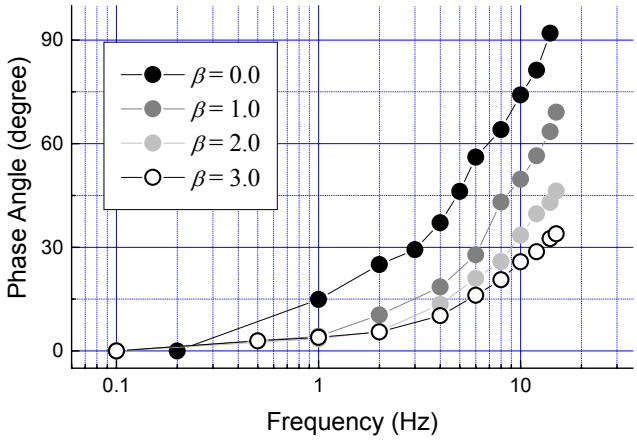

(b) phase lag

Fig. 5.8 Effect of feed-back gain on shaking-table transfer function

5.4. EXPERIMENTS

5.4.1 *Flexible upright cantilever*

In order to provide a proper perspective on the usefulness of the present method, a simple example of simulation of soil-structure interaction effects is introduced herein. Eight steel plates (2000 mm × 300mm × 1 mm) were fastened together with rivets arranged in a grid to form a simple cantilever. The cantilever was then fixed upright on a shaking table with six degrees of freedom, as shown in **Fig. 5.9**[9], because it was expected that the bending of the cantilever would cause a rocking motion in its foundation. The feedback gains, β, of the servo-amplifier for this shaking table are set at 0.53 and 0.41 in respect to horizontal and rocking degrees of freedom. Mechanical

Fig. 5.9 Upright beam on shaking table

Table 5.1 Parameters of cantilever

width (m)	Height (m)	thickness (m)	Bending stiffness *EI* (Nm^2)	density ρ (kg/cm^3)
0.3	1.8	0.008	2132.5	0.00801

Table 5.2 Soil properties

Density ρ_s (kg/cm^3)	shear wave velocity v_s (m/s)	Poisson's ratio ν
0.0016	4.8	0.5

Table 5.3 Parameters for foundation

Radius r_0 (m)	thickness *d* (m)	density ρ_c (kg/cm^3)
0.8	0.1	0.0025

properties of the cantilever are listed in **Table 5.1**. The cantilever is rather flexible, with its natural frequency set approximately at 1Hz, so that interaction forces (both shear force p_x and moment p_θ) are easily measured by bonding strain gages to the lower end of the cantilever. This flexible cantilever was assumed to be mounted virtually on a circular rigid mat foundation (radius (r_0) = 1.2 m, thickness (d) = 0.2 m, **Table 5.3**) resting on a soft semi-infinite half-space of soil ($v_s = 9$ m/s, **Table 5.2**). Meek and Wolf[6), 7)] have developed a unified approach for soil-structure interaction analysis by using truncated semi-infinite cone models representing an unbounded soil medium. According to their approach, the soil supporting a rigid mat foundation is idealized for each degree of freedom as a truncated semi-infinite elastic cone with its own apex height z_0 (**Fig. 5.10**). They also showed that the stiffness parameters for sway and rocking motions are approximated by those of discrete element models illustrated in **Fig. 5.10**. The flexibility, $H_{xx}(s)$, of the discrete-element model in horizontal x direction is described as:

$$H_{xx}(s) = \frac{1}{sC_x + K_x} \tag{5.16}$$

where,

$$K_x = \frac{\rho_s v_s^{\,2} \cdot \pi r_0^{\,2}}{z_0} \tag{5.17a}$$

$$C_x = \rho_s v_s \cdot \pi r_0^{\,2} \tag{5.17b}$$

and v_s is the shear wave velocity propagating through the cone that dominates the stiffness within considerably high frequency range. The apex ratio z_0 / r_0, or the opening angle of the cone, is determined by simply equating the static stiffness coefficient of the disk on the semi-infinite soil half-space to that of the corresponding cone, and is given by:

$$\frac{z_0}{r_0} = \frac{\pi}{8}(2 - \nu) \tag{5.17c}$$

As far as the rocking motion of the disk is concerned, a rotational cone should be discussed. The flexibility, $H_{\theta\theta}(s)$, of the equivalent-discrete-element model in rocking motion is described as:

$$H_{\theta\theta}(s) = \frac{\dfrac{1}{C_\theta}s + \dfrac{1}{M_\theta}}{s^2 + \dfrac{K_\theta}{C_\theta}s + \dfrac{K_\theta}{M_\theta}} \tag{5.18}$$

where,

$$K_\theta = \frac{3\rho_s v^2 I_0}{z_0} \tag{5.19a}$$

$$C_\theta = \rho_s v I_0 \tag{5.19b}$$

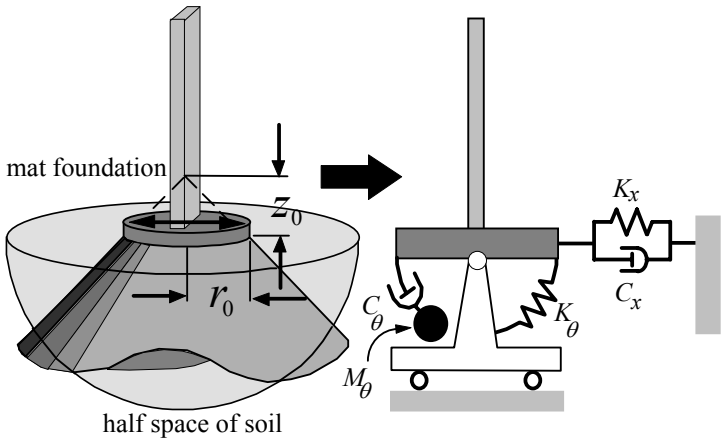

Fig. 5.10 Mat foundation and equivalent discrete element model

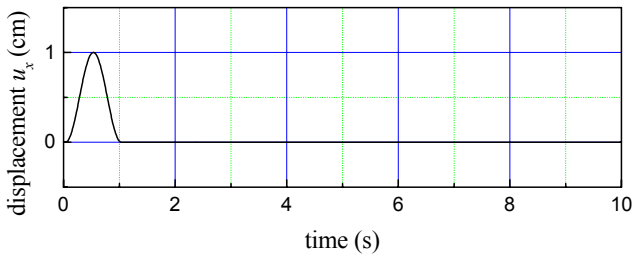

Fig. 5.11 Input base motion $u_x^f + u_x^s$

$$M_\theta = \rho_s z_0 I_0 \tag{5.19c}$$

with $$I_0 = (\pi/4) r_0^{\,4} \tag{5.19d}$$

The velocity v is assumed to be identical to that of the longitudinal wave traveling through the cone when Poisson's ratio of the soil is less than 1/3. For larger values of Poisson's ratio, v is set at $2v_s$. The apex ratio z_0 / r_0 of the rotational cone is:

$$\frac{z_0}{r_0} = \frac{9\pi}{32}(1-\nu)\left(\frac{v}{v_s}\right)^2 \tag{5.19e}$$

In actuality, the lateral and rocking motions of a foundation are coupled, and the present method illustrated in **Fig. 5.1** allows the effect of the coupling to be simulated. The coupling effect, however, is ignored in this simulation. Equations (5.16) and (5.17) indicate that the present example is described by equation (5.4) with *m* set at 2.

As has been mentioned, electric-resistance strain gages were used as a sensing device for both shear-force and moment. A pair of strain gages were bonded on both sides of the lower end of the cantilever to sense the strain in the cantilever resulting from the bending motion of the cantilever. The outputs of strain gages are then connected to an

appropriate bridge circuit that produces a signal proportional to the bending moment. Another pair of strain gages were then pasted 10 cm above them, and the measurement of moments at these two points permitted a determination of the shear force at the lower end of the cantilever. It is noted that the moment and the shear force sensed by these strain gages are not identical yet to the interaction forces, p_x and p_θ, on the soil-foundation interface. The interaction forces are to be evaluated taking into account the inertia forces of the foundation virtually resting on the half-space of soil. For this evaluation, both lateral and rocking accelerations, $\ddot{u}_x$ and $\ddot{u}_\theta$, were measured on the shaking table, and the signals of $\ddot{u}_x$ and $\ddot{u}_\theta$ were multiplied respectively by the foundation mass, M_x $(=\rho_c \cdot \pi r_0^{\,2} d)$, and the moment of inertia, M_p $(=\rho_c I_0 d + M_{trap})$, where M_{trap} is the contribution of the soil mass caught beneath the foundation, and is given by:

$$M_{trap} = 1.2\left(\nu - \frac{1}{3}\right)\rho_s I_0 r_0 \tag{5.20}$$

A horizontal impulse shown in **Fig. 5.11** was given to the shaking table as an effective foundation input motion, $u_x^f + u_x^s$, and the acceleration response at the top end of the cantilever was measured. The dotted line in **Fig. 5.12a** shows the acceleration time history without the interaction motions, u_x^r and u_θ^r, being added; whereas the dotted line in **Fig. 5.12b** shows the response affected by the interaction motions. Thick lines in these figures show the computed responses of the discrete element model in **Fig. 5.10**. In this numerical simulation, the finite difference method was utilized to obtain the solutions in the time domain. The thick and dotted lines are in good agreement in both figures; this fact clearly demonstrates that, for the simulation of soil-structure interaction motions, the present method works properly as expected. These figures show that incorporating the effect of the interaction motion leads to the increase of damping and to the slight decrease of natural frequency as well. Although only horizontal base motion was given to the shaking table, bending motion of the cantilever eventually caused the shaking table (the virtual foundation) to rock as shown in **Fig. 5.13**. The observed rocking motion, u_θ^r, is also in good agreement with the numerical simulation (thick line).

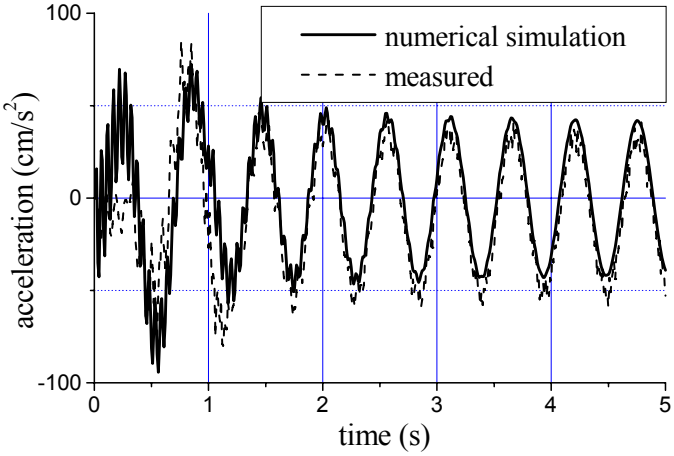

(a) without interaction

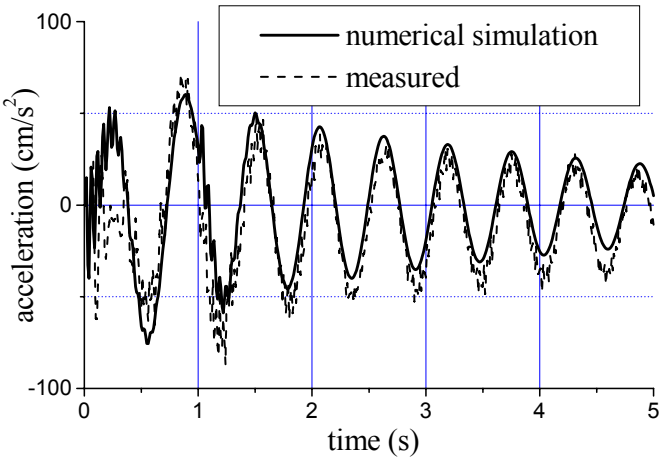

(b) with interaction

Fig. 5.12 Accerelation at the top end of upright beam

The present system is conditionally stable as is often the case with feed-back control systems. Especially when a structure model with low damping ratio is shaken, the motion of the shaking table sometimes echoes through the circuit causing a serious clattering (howling) of the table. **Fig. 5.14** shows one example of clattering that happened before the table was properly heated up and stabilized. The predominant frequency of the noise is 11 Hz, and is about identical to the fourth natural circular frequency of the model. When the predominant frequency is higher than the frequency range in which the desired signal exists, a low-pass filter may be used to reduce the noise. It is however noted that the use of a low-pass filter causes the response of the table to be more delayed. Some built-in device such as an adaptive echo canceller[10] would be useful for further improving its performance.

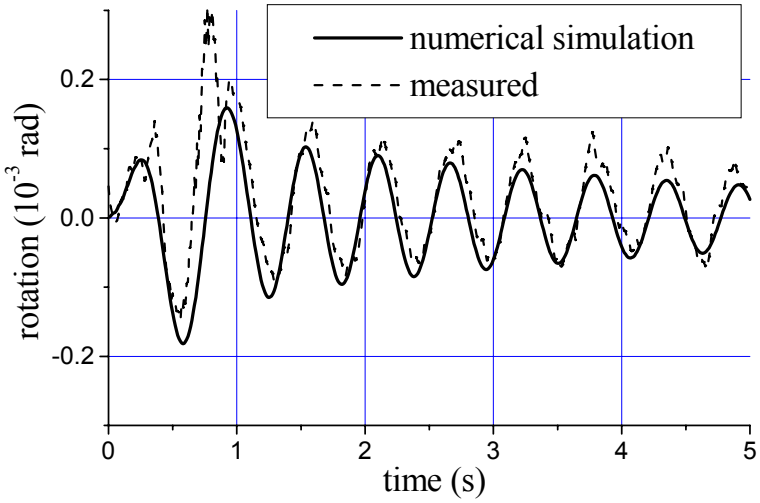

Fig. 5.13 Rocking of shaking table

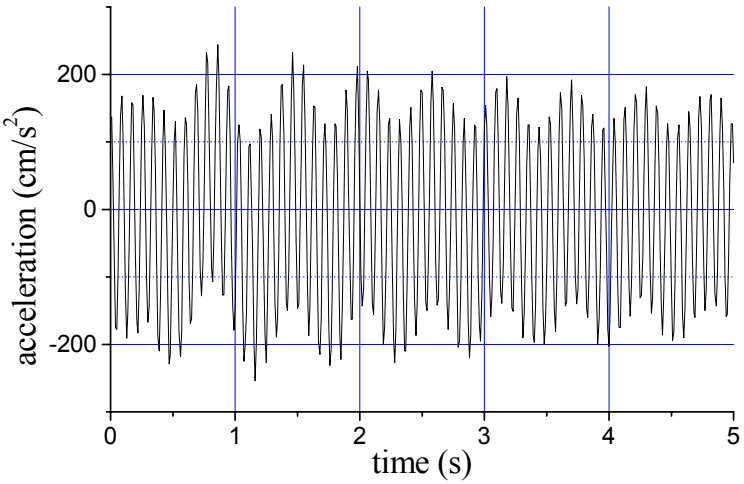

Fig. 5.14 Howling observed at the top end of upright beam

5.4.2 *Slippage of rigid block on mat foundation*

A rigid cylindrical block is assumed to be put on a rigid and circular mat foundation resting on a semi-infinite half medium of soil (**Fig. 5.15a**)[2]. The dimensions of both the prototype block and foundation are listed in **Table 5.4**, whereas **Table 5.5** shows the parameters for the soil medium. Poisson's ration of the soil was set at 0.5 on the assumption that the ground is an alluvial soft soil deposit that is totally saturated with water. In this case also, the soil supporting a circular mat foundation is idealized for each degree of freedom as a truncated semi-infinite cone (**Fig. 5.15b**) with its own apex height z_0. Only translational motion of the foundation is discussed herein, and the soil-foundation is modeled by a damped one-degree-of-freedom system. The model of the soil-structure system is then prepared by reducing the parameters, m, k and c to the uniform scale of 1 to 100. Since the ratio of these parameters is kept unchanged, the time scale is not changed at all.

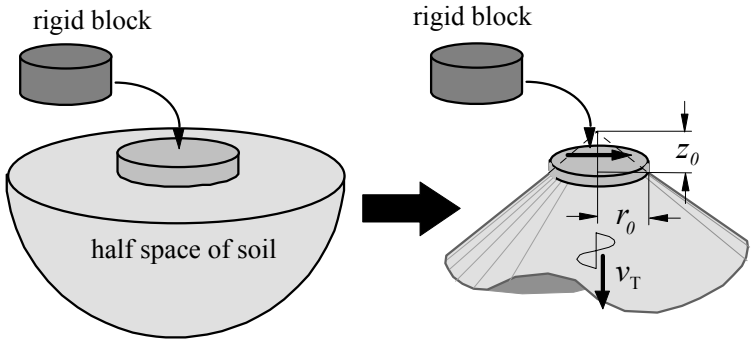

a Rigid block on mat foundation **b** translational cone

Fig. 5.15 Rigid block put on a rigid mat foundation resting on a semi-infinite soil medium

Table 5.4 Dimensions of block and foundation

(a) block

Mass	Radius	height
7.1×10^5 kg	7 m	2 m

(b) mat foundation

Mass	Radius	height
1.4×10^6 kg	11 m	1.6 m

Table 5.5 Mechanical properties of soil

Density	Shear wave velocity	Poisson's ratio
1.6×10^3 kg/m^3	100 m/s	0.5

Fig. 5.16 shows the model put on a shaking table. The steel block in the middle is the model of the rigid block, and the shaking table itself virtually represents the motion of the mat foundation on the semi-infinite soil half-space. The block is put not directly on the shaking table but on a flat steel plate supported by four stiff upright legs with strain gages pasted on them. These gages pick up the base shear force from the block. An impulse as shown in **Fig. 5.17** is given to the shaking table as an input motion u_x. The test was also conducted for the above block model put on the rigid base. **Fig. 5.18** shows time histories of both the displacement of the shaking table and the distance that the block has slipped. Dotted lines in this figure show the motions without the interaction effect being taken into account, whereas thick lines show the motions affected by the soil-structure (foundation-block) interaction. Incorporation of the soil-structure interaction leads to slight increase in the duration of the base motion and drastic decrease of the distance that the block has slipped. The mass of the block is the direct cause of the increase in the duration of the base motion, and the decrease of the sliding distance is closely linked with the increase of the energy that has dissipated as outwardly propagating waves into the virtually spreading soil medium. The present method allows both influx E_{input} and efflux $E_{dissipated}$ of energy through the foundation to be measured in real time. These two kinds of energy are respectively:

$$E_{input} = \int_0^t \left(p_x \dot{u}_x + p_\theta \dot{u}_\theta \right) \cdot dt \tag{5.21a}$$

$$E_{dissipaed} = \int_0^t \left(- p_x \dot{\tilde{u}}_x - p_\theta \dot{\tilde{u}}_\theta \right) \cdot dt \tag{5.21b}$$

The energy, $E_{consumed}$, used up within the model on the shaking table is then obtained as:

$$E_{consumed} = E_{input} - E_{dissipated} \tag{5.21c}$$

Fig. 5.19a shows the variations of these energies with time where the interaction effects are ignored, and thus, the cumulative loss of energy through friction ends up to be the same amount as the energy influx. On the other hand, **Fig. 5.19b**, in which soil-structure interaction effects are incorporated, shows that a part of influx energy dissipates away and just the remainder is used up through friction.

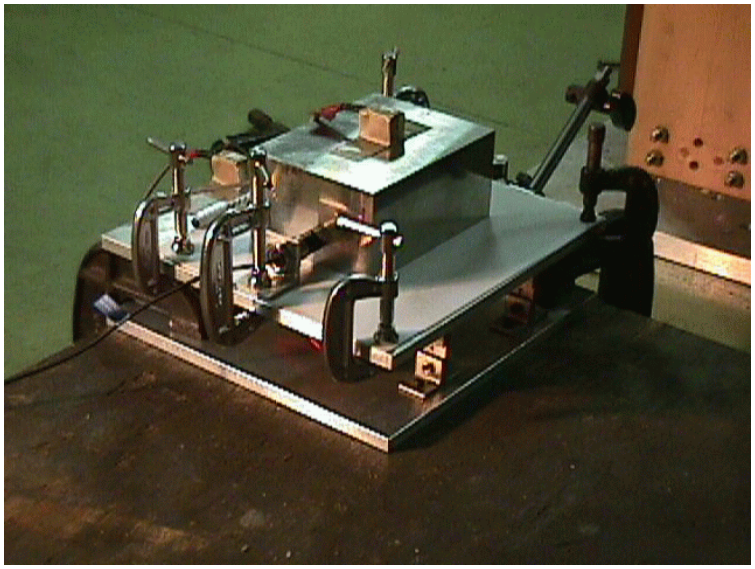

Fig. 5.16 Block model on shaking table

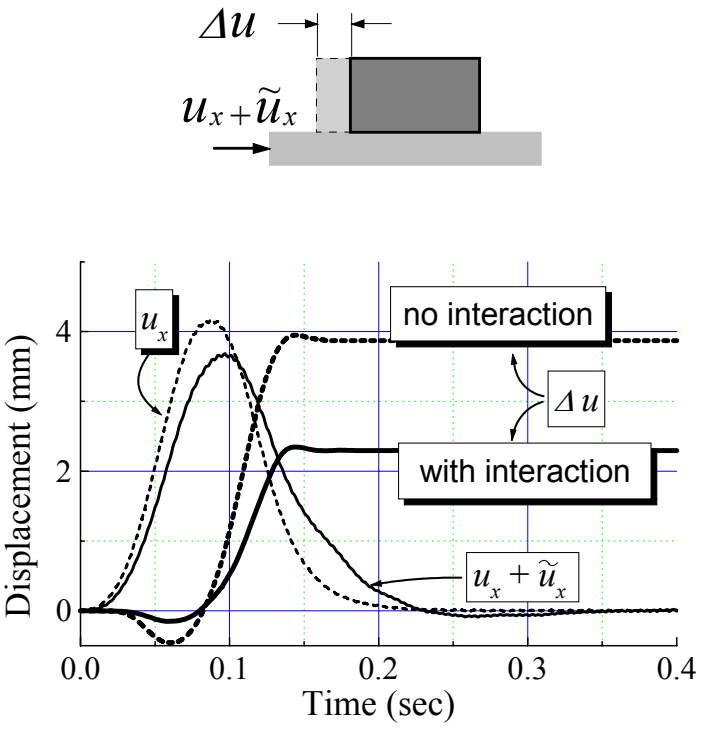

Fig. 5.17 Displacement of shaking table and distance that block has slipped

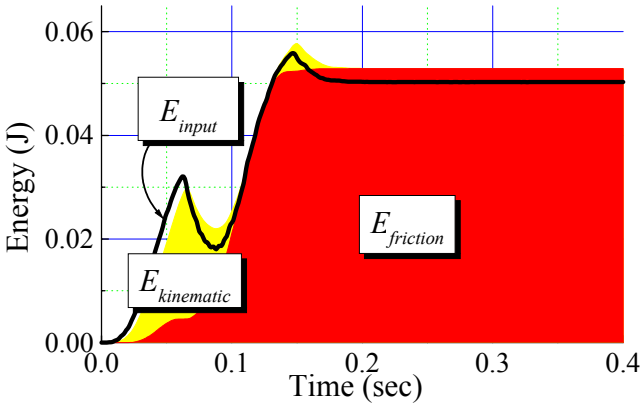

(**a**) no interaction

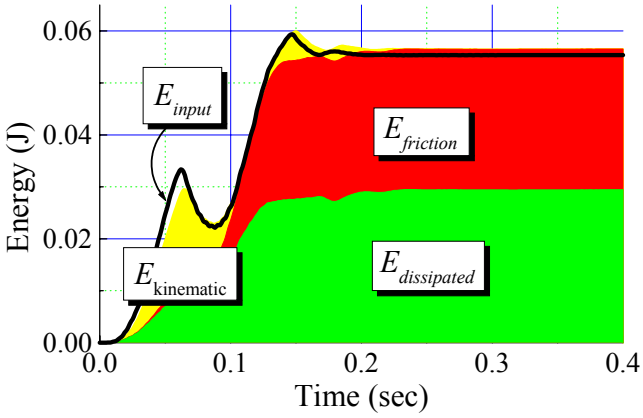

(**b**) with interaction

Fig. 5.18 Influx, efflux and consumption of energy

5.5 SUMMARY

A new method for a model experiment on a shaking table has been presented. The present method allows soil-structure interaction to be simulated. The conclusions of this study are summarized as follows:

(1) In the present method, soil-structure interaction effects are simulated by adding appropriate soil-structure interaction motions to the free-field ground motions at the shaking table. A variety of unit-impulse response functions of bases or soil mediums overlaid with structures are closely approximated by summing up basic functions which can be generated by simple analog circuits and/or digital signal processors. This method

thus has the potential to be applied to a variety of experiments of soil-structure interaction without preparing any physical soil model.

(2) The present system is realized on condition that a shaking table produces faithfully its input motion. The motion produced by the shaking table, however, is not exactly identical to the intended time history because the ratio of output-to-input amplitude of the system does not remain the same over the frequency range desired. The performance of the system's transfer function is also affected by the presence of a model on the shaking table, a fact that may cause the motion of the table to further deviate from the input. This effect will be canceled by multiplying the flexibility function, H, of a soil-foundation system by the inverse transfer function, T^{-1}, of the shaking table system. This manipulation, however, leads to reducing both the mass, M, and the viscous damping coefficient, C, making up the discrete element model equivalent in mechanical properties to the soil-foundation system. Needless to say, the reduced mass, $M - \Delta M$, and the damping coefficient, $C - \Delta C$, must be positive. The conditions are usually satisfied in reality for many cases of soil-structure interaction because wave radiation from a foundation leads the motion of the structure to be noticeably damped. If not, it would be necessary for the time delay to be minimized. One possible measure for reducing the time delay is to increase the feedback gain of a servo-amplifier of the shaking table. It is, however, noted that the increase of feedback gain leads to a decrease in the margin for unstable clattering of the table that is caused by the noise echoing through the closed circuit of the servo-amplifier.

(3) In order to provide a proper perspective on the usefulness of the present method, a simple upright 2,000 mm long steel cantilever was shaken on a shaking table. The observed responses of the beam showed that incorporating the effect of the interaction motion leads to the increase of damping and to the slight decrease of natural frequency as well. The numerical simulations were in good agreement with the observed responses, demonstrating that the present method for the simulation of soil-structure interaction motions works properly as expected. It is, however, noted that unexpected noise amplification can cause serious problem in operating the shaking table when a less-damped structure model is tested on a shaking table.

(4) A steel block was put on a shaking table that virtually represents the sway motion of a rigid circular mat foundation on a semi-infinite half space of soil. An impulsive displacement was then given to the shaking table as an input free-field motion, and both the displacement of shaking table and the distance that the block slipped were measured. Incorporation of the soil-structure interaction led to slight increase in the duration of the base motion and noticeable decrease of the distance that the block

slipped.

REFERENCES

1) Konagai, K., T. Nogami, T. Katsukawa, T. Suzuki and A. Mikami: Real Time Contril of Shaking Table for Soil-Structure Interaction Simulation, *Jour. of Structural Mechanics and Earthquake Engineering, JSCE,* **598/I-44**, 203-210, 1998 (in Japanese).

2) Konagai, K., O. Uemura, T. Katsukawa and T. Suzuki: Real Time Simulation of Soil-Structure Interaction Effects on Shaking Tables, *Proc., 10th Japan Earthquake Engineering Symposium*, **E1-13**, 1647-1652, 1998.

3) Konagai, K. and T. Nogami: Simulation of Soil-Structure Interaction on a Shaking Table, "Numerical and Physical Modeling for Dynamic Soil/Structure Interaction Phenomenon", *Geotechnical Special Technical Publication*, *ASCE*, **64**, 91-106, 1997.

4) Konagai, K. and T. Nogami: Analog Circuits for Simulating Soil-Structure Interaction on a Shaking Table, *Intrn. Jour., Soil Dynamics and Earthquake Engineering*, **17(5)**, 279-287, 1997.

5) Kanya, A. M. and E. Kauzel, Dynamic Behavior of Pile Groups, *Proc., 2nd International Conference on Numerical Methods of Offshore Piling*, Austin, TX, pp. 509-532, 1982.

6) Meek, J. W. and Wolf, J. P.: Cone models for homogeneous soil, *J. geotechnical eng., ASCE*, **118(5)**, pp. 667-685. 1992.

7) Meek, J. W. and Wolf, J. P.: Cone models for embedded foundation, *J. geotechnical eng., ASCE*, **120(1)**, pp. 60-80, 1992.

8) Zadeh, L. A. and C. A. Desoer: *Linear System Theory*, McGraw-Hill Book Co., 1963.

9) Konagai, K. and Katsukawa, T.: Real time control of a shaking table for soil-flexible structure interaction, *Bull., Earthquake Resistant Structure Research Center*, IIS, Univ. of Tokyo, **30**, pp. , 1997.

10) Sondhi, M. M.: An Adaptive Echo Canceller, Bell Syst. Tech. Jour., 46(3), p.497, 1967.